MOLECULAR SIMULATION STUDIES FOR THE TEMPLATED SYNTHESIS OF ULTRATHIN METAL NANOWIRES IN ZEOLITES

By
Javier A. Huertas-Miranda

A dissertation submitted in the partial fulfillment of the requirements of a

DOCTOR OF PHILOSOPHY
in
CHEMICAL ENGINEERING

UNIVERSITY OF PUERTO RICO
MAYAGÜEZ CAMPUS
2012

Approved by:

_____	_____
Arturo J. Hernández Maldonado, PhD Member, Graduate Committee	Date
_____	_____
Carlos Rinaldi Ramos, PhD Member, Graduate Committee	Date
_____	_____
María Curet Arana, PhD Member, Graduate Committee	Date
_____	_____
María M. Martínez Iñesta, PhD President, Graduate Committee	Date
_____	_____
Marco A. De Jesús, PhD Graduate Committee Representative	Date
_____	_____
Aldo Acevedo Rullán, PhD Chairperson of Department	Date

Table of Contents

List of Figures

List of Tables

Acknowledgments

In the first place, I would like to thank Dr. Julio Briano who *persuaded* me to continue graduate studies in the Department of Chemical Engineering at the University of Puerto Rico at Mayagüez. I would also like to thank professor Héctor López (Departmental Director), Dr. John Fernández van Cleve (former Dean of the College of Agricultural Sciences), and Dr. Héctor Santiago Anadón (former Dean of the Agricultural Experiment Station), all who authorized and encouraged my participation in the graduate studies program, while permitting me to continue with my tasks as professor at the Agricultural and Biosystems Engineering Department and the Food Science and Technology Program.

I acknowledge the Chemical Engineering Department of the University of Puerto Rico, the NSF founded Institute of Functional Nanomaterials, and the SLOAN Foundation for their financial support. I am also grateful for the support, advice and assistance of Dr. Yasuyuki Ishikawa of the Chemistry Department of the University of Puerto Rico at Río Piedras, and his former graduate student Dr. Juan Santana.

Special thanks to Leonel, Angel, Lilliana, Héctor, and Jennie (members of our research group) who gave me great advice during the practices of my oral presentations. Also thanks to my friend Misael Díaz, who read and revise my dissertation proposal.

Finally, I would like to thank the members of my graduate committee, especially to Dr. María M. Martínez Iñesta, who adopted me as her graduate student. She was very patient and supportive during these years and was always there when I needed her advise.

Abstract

In the present work geometric optimizations, Metropolis Monte Carlo, and molecular dynamics simulations were done to study the feasibility of synthesizing Ni and Pt nanowires inside the pores of one dimensional zeolite frameworks. Conditions studied included different frameworks (cancrinite (CAN) and mordenite (MOR)), metal concentrations, silicon to aluminum ratios (Si/Al), and temperatures. It was found that the formation of metal nanowires is influenced by all these parameters.

In general, larger sizes of interconnecting windows between main pore channels and side pockets (which is the case of MOR) could have a detrimental effect in the formation of nanowires inside zeolites. This effect can be reduced with the use of low Si/Al which can promote the displacement of guest metal atoms from the side pockets to the main pore channels, where metal nanowires could be formed. High metal concentrations also promote the migration of metal atoms to the pore channels, as well as the formation of elongated nanostructures. If these variables are managed adequately, an increase in temperature has a positive effect in the formation of metal nanowires because it increases the mobility of guest metal atoms

The viability of forming stable one dimensional Pt structures inside the pores of Virginia Polytechnic Institute Eight (VET) - type zeolites was also evaluated by using the above mentioned molecular simulations techniques, as well as grand canonical Monte Carlo. The resulting nanostructures were optimized and analyzed as formed both inside and outside of the zeolite template. The results show that theoretically it is possible to form relatively thermally stable ultrathin nanowires, when synthetized at a low Si/Al ratio

and a high temperature. The results also show that the stable Pt nanowire structure obtained with the *pcff* forcefield was qualitatively similar to the one obtained with DFT.

Resumen

En el trabajo que se presenta a continuación, se realizaron optimizaciones geométricas, y simulaciones de Metropolis Monte Carlo y de dinámica molecular para estudiar la viabilidad de sintetizar nanocables de Ni y Pt dentro de los poros unidimensionales de zeolitas. Las condiciones estudiadas incluyeron el uso de distintos armazones de zeolitas (cancrinita (CAN) y mordenita (MOR)), concentraciones de metales, razón de silicio y aluminio (Si/Al), y temperaturas. Se encontró que la formación de nanocables metálicos está influenciada por todos estos parámetros.

En general, el mayor tamaño de ventanas de interconexión entre los canales de poro principal y bolsillos laterales (que es el caso de MOR) podría tener un efecto perjudicial en la formación de nanocabes dentro de zeolitas. Este efecto puede reducirse con el uso de una baja razón de silicio a aluminio (Si/Al), lo cual promueve el desplazamiento de átomos metálicos de los bolsillos a los canales de los poros principales, que son los lugares donde podrían formarse nanocables metálicos. Las altas concentraciones de metales también fomentan la migración de estos átomos a los poros de la zeolita, así como la formación de nanoestructuras alargadas. Si estas variables se manejan adecuadamente, un aumento de temperatura tendrá un efecto positivo en la formación de nanocables pues aumenta la movilidad de los átomos metálicos y por lo tanto la posibilidad de interactuar entre ellos y formar estas estructuras.

En adición, se evaluó la viabilidad de formar estructuras unidimensionales estables de Pt dentro de los poros de zeolitas del tipo Instituto Politécnico de Virginia Ocho (VET), utilizando las técnicas de simulación molecular mencionadas anteriormente,

así como simulaciones de Monte Carlo en el conjunto gran canónico. Las nanoestructuras resultantes se optimizaron y evaluaron tal como se formaron dentro de la plantilla de la zeolita y luego de su remoción de esta. Los resultados muestran que teóricamente es posible formar nanocables ultra delgados con relativa estabilidad térmica en la zeolita VET, si estos se sintetizan a Si/Al bajos y altas temperaturas. Los resultados también muestran que la estructura más estable de Pt obtenida con el campo de fuerza *pcff* es similar, cualitativamente hablando, a la obtenida después de optimización geométrica con DFT.

Chapter 1 - Introduction

1.1 Ultrathin Metal Nanowires

Nanotechnology is one of the most promising fields of science and engineering. It has potential to benefit mankind with the creation of new materials, devices, and systems with novel properties. [1] This field is mainly about the creation, study and uses of nanoparticles, which are particles with at least one dimension smaller than 100 nm. [2] The range of potential uses of nanoparticles is ample and includes diverse applications such as drug and gene delivery, [3,4] cancer treatment, [5,6] biosensors, [7] reaction catalysis, [8] and electronic data storage. [9]

Nanoparticles have received substantial attention from the scientific community because of their unusual and interesting physical properties. For example, gold nanoparticles in solution can scatter visible light instead of absorb it, presenting unusual colors such as deep red or black. [10] These nanoparticles are also effective catalysts while in the bulk gold is inert. [11] Property changes of nanoparticles, with respect to those of bulk materials, are mainly due to the fact that, at the nanometer scale, the fraction of atoms on the surface is greater than for particles of larger size. Because of the relation between nanoparticle's size and its uncommon properties, it is an active area of research to synthesize them with the smallest possible size. [12]

There are many types of nanoparticles which can be classified according to their size, shape, and composition. [13] Our interest is on ultrathin metal nanowires, which are one-dimensional structures with no empty cores and with diameters of less than 10 nm. [14] These particles have the potential to be used in applications such as catalysis, [11,

15] sensor applications, [16,17] and very small electronic circuits. [17] Unusual properties of ultrathin nanowires include, among others,: quantum conductance, [18] low thermal conductivity such as in Si and Ge alloys nanowires, [19] ferromagnetism in Pt and Pd nanowires, [20] and negative magnetoresistance, [21] such as in Bi nanowires. [22]

1.2 Templated Synthesis of Metal Nanowires

The methods to synthesize metal nanowires make use of certain techniques such as ligand control, oriented attachment, and the use of templates. A review of these and other techniques for the synthesis of metal nanowires and other nanostructures is available elsewhere. [14,23]

This dissertation focuses on the templated synthesis, a convenient and well documented technique in which certain materials help to provide control over the size and shape of metal nanowires during the growth of these particles. When compared with other techniques, the templated synthesis has the advantage of yielding more monodisperse nanowires.

The methods that make use of templates for the synthesis of metal nanowires include the infiltration of molten materials, [24] supercritical inclusion, [25-28] and impregnation of metal-salt solutions [29-30] in porous materials such as mesoporous materials and zeolites. Other methods are vapor-liquid-solid (VLS) reaction using nanocrystals [31] and micellar growth. [32]

Materials that can be used as templates for the synthesis of metal nanowires include nanocrystals [31,33,34-36], mesoporous materials [25-30,37], inorganic polymer templates [38,39] and zeolites [24,40]. Among them, mesoporous materials are one of the most successful templates used for synthesis of metal nanowires. [41-49] These materials are highly ordered structures with pore sizes between 1.5 to 40 nm. Using these templates copper, [41] gold, [42,43] palladium, [44-45] rhodium [46] and platinum [47-49] nanowires have been synthesized, with diameters ranging between 2.5 to 20 nm.

An alternative as templates for the synthesis of ultrathin metal nanowires are zeolites with one dimensional pore channels such as cancrinite, mordenite and Virginia Polytechnic Institute Eight (VPI-8), with the CAN, MOR and VET structural frameworks, respectively. These materials have small pores with diameters ranging between 0.4 to 1.3 nm, which can be theoretically used to cast ultrathin metal nanowires.

In the next section the composition, structures, and properties of zeolites are discussed, as well as some research work related to the use of these materials in the synthesis of ultrathin metal nanowires.

1.3 Zeolites and Their Use as Templates

Zeolites are crystalline aluminosilicate materials commonly found in nature, whose discovery in 1756 is attributed to Alex Fredrick Cronsted, a Swedish mineralogist. Cronsted coined the word *zeolite*, which based on its etymological origins (in Greek) means *boiling stone*. The name was given by Cronsted because of his observations with

stilbite, a mineral that lost considerable amounts water in the form of vapor when heated. [50]

The commercial uses of zeolites are broad and include, among others, purification and softening of water, [51] separation of specific compounds such as CO_2, SO_2 and N_2 in gaseous mixes, [52] catalytic cracking in petroleum industry, [53] soil treatment [54] animal nutrition, [55] and removal of fission products in nuclear waste. [56] It has also been used as an additive in detergents, [57] and asphalt concrete. [58] A review of the many applications of zeolites is available elsewhere. [59] The variety of uses for zeolites is due mainly to the properties of these materials, which include the ability to selectively adsorb molecules on a size exclusion process and to interchange a wide variety of ions. These properties are intimately related to their internal structure and pores sizes.

Typically, zeolites are composed of Si, Al, and O atoms. Each Si and Al atom in the zeolite framework is connected to four oxygen atoms in a tetrahedral configuration. In this arrangement Si^{4+} cations are charged balanced with the corresponding O anions. In the case of Al^{3+} cations, however, it results in net negative partial charge that can be balanced by extra-framework cations such as Na^{+}, K^{+}, Ca^{2+} or H^{+}; the later being commonly used to provide the necessary Bronsted acidity for zeolite's applications in catalysis. The ratio of Si atoms to Al atoms (Si/Al) can vary from infinite to one, depending on the zeolite structure and the synthesis process. Si/Al values lower than one are not favored energetically because of the high electrostatic repulsion of Al atoms in adjacent tetrahedrals.

The Si and Al tetrahedrons are interconnected in a unique arrangement of atoms for each framework type, forming cavities or channels with pore diameters ranging

between 0.4 to 1.3 nm. Depending on the framework type, zeolite pores can be interconnected; thus these materials can have one, two or three dimensional pore channels.

There are over 200 zeolite frameworks, of which about 40 of them can be found in nature and the others have been artificially synthesized. More information about these and other zeolite frameworks is available at International Zeolite Association (IZA) Structure Commission Website. [60] Key examples of these are given in Figure 1.1.

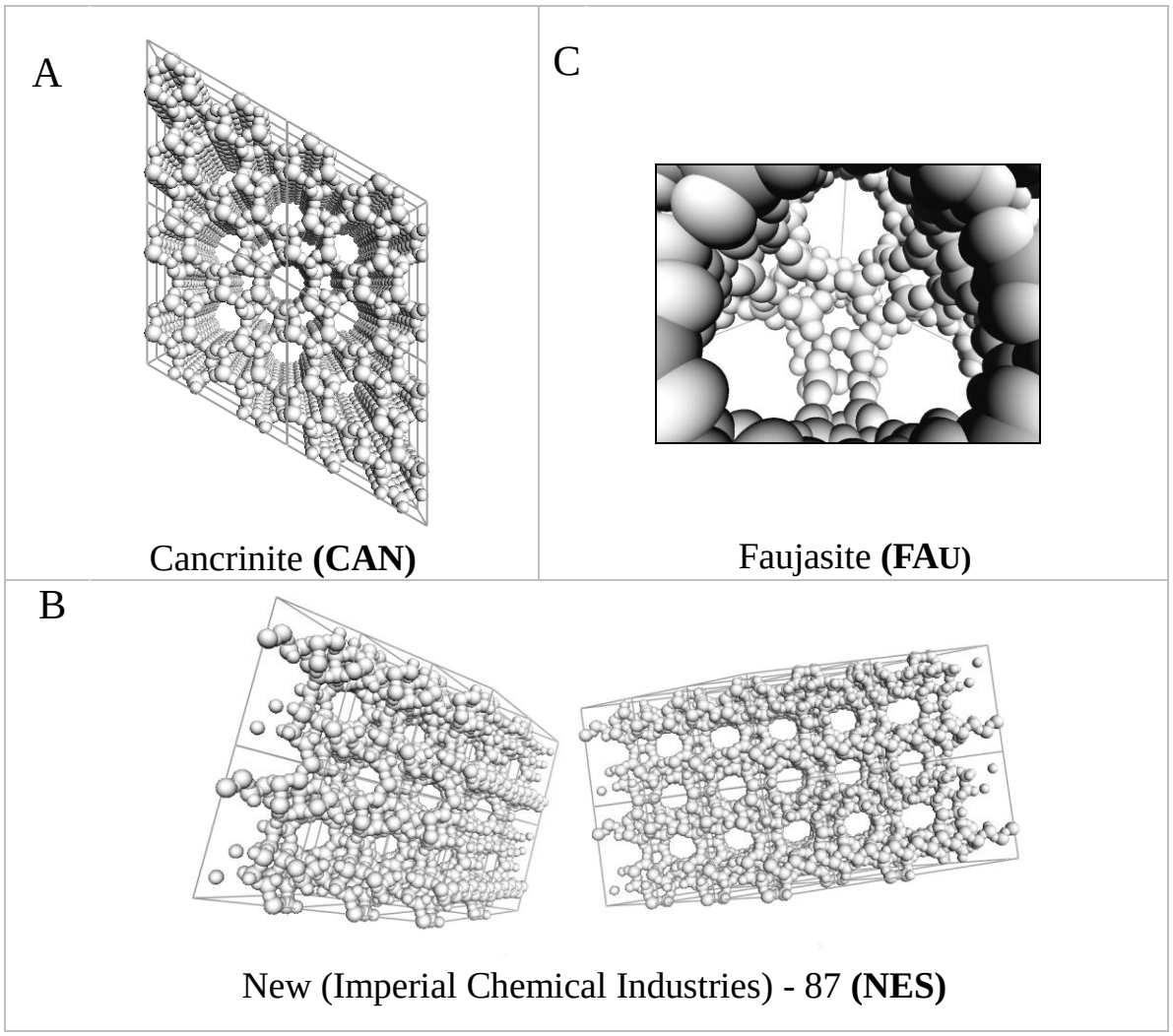

Figure 1.1 - Examples of zeolites with one (A), two (B), and three (C) dimensional pore frameworks

The use of zeolites as templates for the synthesis of metal nanoparticles has been studied and promising results have been obtained for 0D clusters. [61,62] However, limited results have been obtained for ultrathin metal nanowires synthesized inside zeolite pore structures. Silicon [63] and silver [64] nanowires have been obtained in zeolites using a disproportionation reaction with thermal evaporation and electron beam irradiation, respectively. With these methods wires grew inside and outside the pores of the zeolites. Similar results were obtained in a study that used an electron beam to irradiate copper containing zeolite, for the production of single crystal copper wires. [65] More recently, Pt nanowires were synthesized on the surface of mordenite granules using the solid state reduction method. [66] A common result in these studies was that the diameter of the reported nanowires was larger than the size of the pores, evidencing the limitations of these synthesis methods in terms of the effective use of the zeolite as a template. A notable exception is Bi, a metallic element considered as a "poor metal"; these nanowires have been effectively synthesized obtaining one-dimensional structures of only two atoms across by infiltrating molten material in zeolite mordenite. [24]

1.4 Motivation and Scope of this Dissertation

As discussed in the previous section, there is a lack of relevant literature on the effective use of zeolites as templates for synthesis of ultrathin metal nanowires. This lack of literature can be attributed to the many variables that affect the templated synthesis process, including those related to the diffusion limitation and electrostatic influence of the zeolite framework. It is reasonable to state that a better understanding of the effect of

these variables will ultimately help researchers to develop methodologies for the effective synthesis of ultrathin metal nanowires in zeolites.

The study of the combined effect of many of these variables using experimental techniques can be overwhelming in terms of cost and time. One effective way to study the effect of these parameters is through the use of molecular simulation techniques. For example, the diffusion of molecules and nanowire stability can be studied using techniques such as molecular dynamics, while the adsorption of molecules inside zeolite pores can be studied using Monte Carlo simulations. In this dissertation, the research work was focused on the study of conditions that promote the formation of ultrathin metallic nanowires in zeolites by means of molecular simulations.

The main objective of this research is to study the behavior of neutral Ni and Pt metal atoms inside zeolites with the one dimensional pore channels using molecular simulations under conditions that simulate the final steps of templated synthesis methods in which ultrathin nanowires could be formed. The idea is to gain a greater insight of the driving principles that describe the suggested process. The study was centered in the effect of zeolite framework, Si/Al ratio, local metal loading, and temperature on the positioning of metal atoms inside the zeolite frameworks and their role in the formation of metal nanostructures inside the pore channels.

In the next chapter, a brief discussion of the molecular simulation tools used in this dissertation is presented. This includes the techniques of geometric optimizations, Monte Carlo simulations, and molecular dynamics. Also a discussion of Density Functional Theory and forcefield methods for the estimation of potential energy of

molecules is presented, as well as theory related to mechanical statistics for the computation of energy of systems at equilibrium.

A literary review of pertinent research works is presented in Chapter 3. Work related to molecular simulations in zeolites and structural stability of nanostructures is included.

In Chapter 4, the effect of metal loading and Si/Al on the positioning of Ni atoms inside CAN and MOR zeolite frameworks is studied. Geometric optimizations and Monte Carlo simulations were used under the canonical ensemble to find the most stable location of Ni atoms. The results presented in this chapter were published in Sensors and Transducers [67] and Molecular Simulation Journals. [68]

Chapter 5 is a study related to the one presented in Chapter 4, but for Pt atoms inside the MOR framework. A similar approach to the one in Chapter 3 was used to determine the most stable places were Pt atoms are positioned inside the MOR framework at different metal loadings and Si/Al conditions, but this study also includes the effect of temperature and the use of molecular dynamics. The dynamic behavior of Pt atoms inside MOR was studied with molecular dynamic simulations using fixed loads of Pt atoms at different Si/Al and temperature conditions. These results were published in Molecular Simulation Journal. [69]

In Chapter 6, the viability of forming stable one dimensional Pt structures inside the pores of VET-type zeolites was evaluated. Monte Carlo simulations under the grand canonical ensemble were used to promote the formation of one dimensional Pt structures within the VET framework. The resulting nanowires were geometrically optimized and analyzed as formed both inside and outside of the zeolite. The unidimensional structures

were also geometrically optimized using DFT and the results compared. The thermal stability of the one dimensional Pt structures formed was also studied using molecular dynamics techniques. This work was submitted to the journal Molecular Simulation Journal and is currently under revision.

Finally, the last chapter includes an analysis, discussion and final conclusions of all the results presented in this dissertation. This chapter also includes recommendations for future studies.

Chapter 2 - Molecular Simulations

In this dissertation, three of the most used and proven techniques for molecular simulations are used: geometrical optimizations (also called energy minimizations), Monte Carlo simulations, and molecular dynamics. In this chapter, these techniques are introduced as well as the common methods used by them to measure energy of particles; i.e., Density Functional Theory and forcefields. Explained as well is the theoretical basis of statistical mechanics which allows total energy computation of systems in equilibrium for both Monte Carlo and molecular dynamics. A more detailed review of these and other techniques and methods can be found elsewhere. [70-73]

2.1 Geometric Optimizations

Geometric optimizations in molecular simulations imply the finding of the coordinates of the atoms of a system that yield the lowest potential energy configuration. When geometric optimizations are done, the final result represents a stable or equilibrium state of a molecular system which corresponds to a global or local minimum on the so-called potential energy surface. During optimization, numerical procedures are employed to move atoms in order to reduce the gradients of potential energy of the system until they become negligible. Geometry optimizations do not take into consideration the effect of temperature during the minimization process. The final state reported from these optimizations represents the configuration of atoms at 0 K.

The process of minimization in geometrical optimization usually requires the evaluation of a function for the potential energy of a system, as well as the first and

second derivatives of this function. As with any other function at a local or global minimum, the first derivative of the potential energy function with respect of each variable is zero (for all inflection points) and the second derivative is positive (which is exclusive of the minima points in which the function interval is concave upward).

There are several numerical methods for minimization that can be used to perform geometric optimization. Two of the most used are the steepest descent and the conjugate gradient. These methods are preferred because they only require the first derivative. This implies less computational demands and faster execution times, which are critical for systems with a large number of atoms. Steepest descent and conjugate gradient change the coordinates of atoms, moving the whole system closer to a minimum point. In both methods, the gradients used to find the minima are orthogonal (or parallel) to the net force. The main difference between the two methods consist in the direction of the movement through the successive steps; while the steepest descent method uses orthogonal vectors for movements, the conjugate gradient uses conjugated directions. In this dissertation the conjugate gradient method was used because it converges faster when the position of atoms are not far away from the local minimum, as it was usually the case in our systems.

Geometric optimizations often confront the problem of identifying points which represents a global minimum. Typically several minimizations are performed at different starting points and comparisons of energy values of the final conformations are used to select the global minimum. Other method widely used is simulated annealing, which combines the use geometric optimizations in a sequence with Monte Carlo or molecular dynamics simulations (explained below) at different temperature intervals where the

system is permitted to reach equilibrium. The variation in temperatures permits to overcome existent energy barriers that circumscribe local minima.

2.2 Monte Carlo Simulations

Monte Carlo molecular simulations, which are based on the principles of statistical mechanics, are preferred over molecular dynamics simulations (explained below) to estimate bulk physical properties of very large systems because they require less computational time.

The most commonly used Monte Carlo method for molecular simulations is the Metropolis Monte Carlo. This method is appropriate only for systems in equilibrium and is used, among others things, to estimate thermodynamical properties and sorption isotherms of gases in porous materials. It is based on a rejection sampling algorithm, created by Nicolas Metropolis, [74] which selects a sequence of samples (events) from a probability distribution (e.g. Boltzmann distribution law). The sequence created is a Markov chain, in which probability of selecting a new state (from a finite number of possible states) only depends on the current state. As the new state of the Markov chain does not depend on a sequence of previous events there is no need to register them, considerably reducing computational resources required in this type of simulation.

The algorithm presented in Figure 2.1 illustrates a typical implementation of Metropolis Monte Carlo. The movement of a randomly selected particle is proposed from a place described by the position vector $\vec{\varepsilon}_o$ to a new place described by $\vec{\varepsilon}_n$, a randomly selected position. The potential energy of the new state $E(\vec{\varepsilon}_n)$, usually

calculated by a forcefield expression (see section 2.4.2), is compared with the one of the previous (or older) state $E(\vec{\varepsilon}_o)$. If the movement represents a decrease in the energy of the state, it is always accepted. If not, a random number between 0 and 1 is generated and compared with the probability that the particle can reach the new position. If the random number is less or equal than the probability, the movement is accepted; if the number is greater than the probability, the movement is rejected. When the movements are accepted, a counter (I) is increased and the value of some accumulative register is altered. Typically, this register is done to estimate thermodynamic properties of the system studied, such as energy, entropy, etc. The contribution of such property for the specific state is added in the register and finally the property is calculated by estimating the mean value based on a density of probabilities.

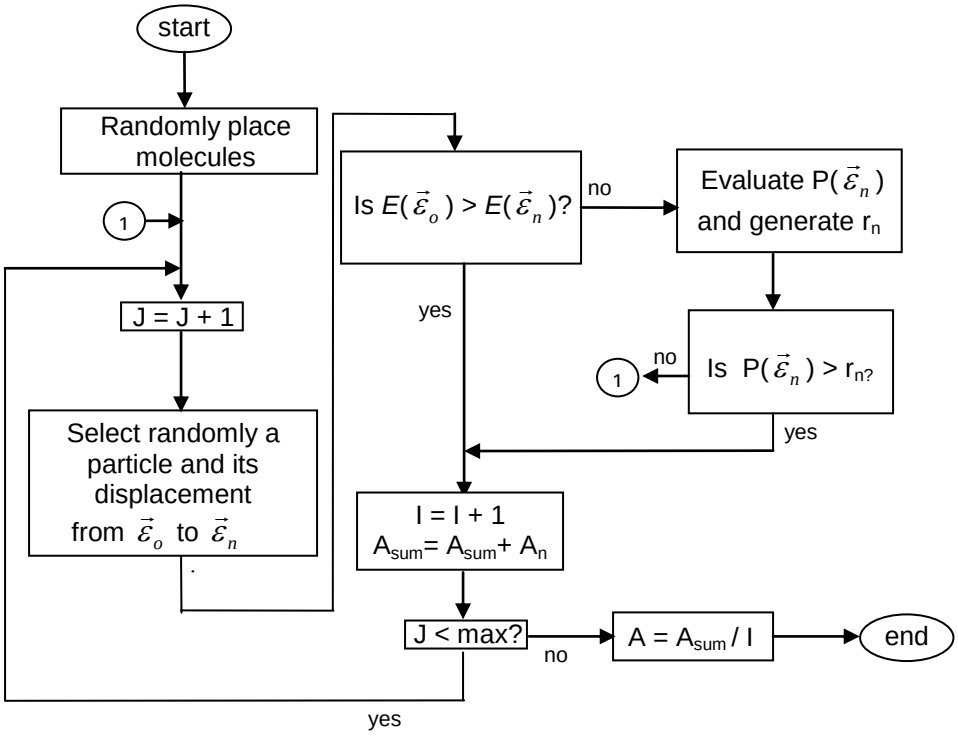

FIGURE 2.1 - Schematic Representation of the Metropolis Monte Carlo Algorithm

As mentioned before, Metropolis Monte Carlo is intended for systems that are in equilibrium. Because of that, before measuring the properties of a system, several equilibration steps are done with the Metropolis algorithm until the mean total energy of the system reaches a constant value. Also, when this method is used to estimate thermodynamic properties, it is expected that the system evaluated satisfies the principle of ergodicity, that is, the system must have the same behavior when the property measured is averaged over time as when it is averaged over space.

The majority of Monte Carlo molecular simulations follow the same algorithm proposed by Nicolas Metropolis. The main differences are on the computation of the probability that a molecule can reach a new position, which depends on the set of properties which are fixed in the system studied during the simulation. For example in the so called canonical ensemble, which is the one used in classical Metropolis Monte Carlo simulations, the fixed properties are the number of moles, temperature, and volume. The grand canonical ensemble is an open system with constant volume, temperature, and chemical potential. The microcanonical ensemble on the other hand is an isolated, closed system with constant energy, volume, and number of moles. The isobaric/isothermal ensemble is an alternative approach, where a closed system with fixed pressure, temperature, and number of moles is used.

2.3 Molecular Dynamics

Classical molecular dynamics simulate the movement of molecules on an individual basis, treating atoms as rigid bodies. Because of that assumption, the

movement of atoms and molecules is described by using Newton's well known equation of force

$$\vec{F}_{net} = \sum_i \vec{F}_i = m\vec{a} \,. \qquad \{1\}$$

Here $\vec{F}_{net}$ is the net force over a specific particle (atom), m and $\vec{a}$ are the net mass and acceleration of that particle, respectively, and $\vec{F}_i$ is the force between the particle and another particle identified with the subscript i. The acceleration vector $\vec{a}$ can be expressed as the second derivative of the position vector with respect to time. Because of that, we have in Newton's law a simple but effective way to describe the motion of particles as a function of time. For a single particle in which Newton's law is applied, the mass term will not represent any trouble; the main issue arises in the estimation of the net force applied to this single particle. This force can be calculated as the gradient of the potential energy (E_{pot}) of the particle:

$$\vec{F}_{net} = -\nabla E_{pot} \qquad \{2\}$$

In order to use effectively these equations, the potential energy of the particle must be estimated. This energy estimation is usually done with forcefields, as discussed below.

Once the energy is calculated, the problem is reduced to solving numerically the systems of equations that describe the movement of the particles. There are several ways to perform this task, but the most commonly used is the one described by the Verlet algorithm. This method resolves directly the Newton equation of motion by estimating the new position of the particle $\vec{r}(t+\delta t)$ for the time step δt, using:

$$\vec{r}(t+\delta t) = 2\vec{r}(t) - \vec{r}(t-\delta t) + \delta t^2 \vec{a}(t). \qquad \{3\}$$

Here $\vec{r}(t)$ is the present position of the particle, $\vec{r}(t-\delta t)$ is the position of the previous iteration, and $\vec{a}(t)$ is the acceleration of the particle. Equation 3 is obtained by the sum of the truncated Taylor expansions that define $\vec{r}(t+\delta t)$ and $\vec{r}(t-\delta t)$; such truncation produces an error of the order of δt^4. [67] By adding these expressions, the velocity terms are canceled. When the velocity is needed, it can be calculated using the expression:

$$\vec{v}(t) = [\vec{r}(t+\delta t) - \vec{r}(t-\delta t)]/(2\delta t). \qquad \{4\}$$

The errors related to the velocity computation on the Verlet algorithm are of the order of δt^2. [70] There are many algorithms that have been proposed to improve the exactness of molecular speed values during simulations over the ones estimated by the Verlet algorithm (e.g. prediction correction methods, leap frog, and velocity Verlet). However, when considering global properties, all these algorithms (included Verlet) have errors of the same order and generate very similar trajectories. [70] The preference of the Verlet algorithm over others is because it is a simple algorithm that is easily implemented and requires less computational time and resources.

2.4 Methods for Energy Computation

2.4.1 Quantum Mechanical Methods

The Latin words *ab-initio* mean "from the beginning". In *ab-initio* methods, energy calculations are performed using the principles of quantum chemistry; the use of empirical data is not allowed. All *ab-initio* methods have their basis on the numerical

nonrelativistic solution of the Schrödinger equation, which describes the space/time dependence of quantum systems.

The first of these methods, developed by Douglas R. Hartree, [75] is a numerical method that approximates wave functions and energies of atoms. The approach used by Hartree was expanded later by Vladimir Fock, [76] with the inclusion of the anti-symmetry principle of the wave function, related to the presence of two electrons in the same quantum state.

During *ab-initio* calculations, wave functions that describe the system are represented by state vectors whose components are linear combinations of certain functions called basis functions; these are selected from the so called basic sets, which are sets of functions that describe atomic orbitals of certain atoms. The first basis sets created were based on the Slater type orbitals, which were introduced by John Slater in 1930. [77] Basis sets based on Slater type orbitals are interesting from a theoretical point of view, but they are not practical for fast calculations. However, Slater type orbitals can be approximated by a linear combination of Gaussian type orbitals; the use of Gaussian orbitals can speed computations between 4 to 5 orders of magnitude when compared with the Slater type orbitals. Among the most used basis sets are the ones created by Pople et al. [78] and the ones from Dunning et al. [79]

Ab-initio methods have the advantage that they can be made to converge to exact solutions. However, for simulations of systems with a large number of atoms they are impractical, due to the large number of computations required. As energy computations in many *ab-initio* methods consider the wave function of each electron and their contribution to the many body wave function, the addition of atoms in a simulation

increases exponentially the time required for computations. In general the time it takes to do these simulations is considered to approximately scale as N^4 were N is the number of basis functions.

A very popular method that is a variant of the *ab-initio* methods is the Density Functional Theory (DFT). This method developed by Hohenberg and Kohn, [80] has its roots on the Thomas-Fermi model. [81] The main idea behind the DFT is to replace the calculation of the many body electronic wave function with the calculation of the overall electronic density distribution of the system. Because the many body electronic wave function is based on a Slater type determinant of N single electron wave functions (with 3N variables) and the electronic density distribution function is only dependent of 3 spatial variables, calculations with DFT are considerably faster than other *ab-initio* methods.

DFT is based on the principle that properties of a system such as ground state energy can be uniquely defined by the electron density. This concept is mathematically expressed by the use of functionals, which are operators that allow functions to be mapped to a number.

While DFT has been used effectively for calculations related to solid state physics since its inception in 1964, it was not until the 1990's that it became a widely used method for quantum chemistry calculations, when the approximations used were improved to estimate exchange and correlation interactions.

2.4.2 Forcefields

Forcefields are parameterized mathematical models designed to estimate the potential energy of molecules. The parameterization of forcefields is usually based on both, first principle calculations (usually DFT) and experimental observations. The energy computations of a system of many molecules are done by adding the estimation of the internal energy of each molecule to the potential energy due to interaction forces between each molecule and other non bonded surrounding particles (atoms or molecules). For the internal potential energy estimations, bonds between atoms are usually considered as cylindrical elements that are submitted to tension, compression, and torsion. These models also consider energy contributions associated with the angle between bonds or contributions related to angular deflection in planar molecules. All these terms are usually treated as harmonic oscillators and typically bond braking is not allowed.

The calculation of potential energy contributions due to non bonding elements can consider interactions between two or more particles; however, pairwise contributions usually have a higher order of magnitude and its precision is enough to justify, in many cases, elimination of the other terms. [70] Because of the complexity and computational time required to include higher order contributions, many forcefields only consider pairwise contributions for estimation of energy contributions by non bonding particles.

The most common pair contributions considered in forcefields are the van der Waals attraction and repulsion forces, and the Coulombic forces between partial charges. The van der Waals contributions due to attraction forces are usually functions of the sixth power of reciprocal distance between particles ($1/r_i^6$). On the other hand, repulsion forces are usually assumed to be functions of $1/r_i^n$, where the value of n is different depending

on the potential model used (e.g. n=12 for Lennard-Jones). Coulombic forces are usually functions of $1/r_i^2$.

Because computations with forcefields use straight forward substitution of the nuclear positions of atoms in their parameterized functions and there is no consideration of the electron contributions in the calculations, they are several orders of magnitude faster than DFT, especially for systems with a large number of atoms. The computational speed of forcefields made them only possible choice for potential energy calculations in simulations that require a large number of iterations using Monte Carlo or molecular dynamics.

In this dissertation, the Polymer Consistent Forcefield (*pcff*) was used for most of the energy computations required in the geometric optimizations, Monte Carlo and molecular dynamics simulations. *Pcff* is a well known and extensively used forcefield developed by Sun et al.. [82-83] It was selected after evaluation of several forcefields because it is parameterized for zeolites as well as 20 inorganic metals (including Ni and Pt which are the metals considered in this study), accounting for the interaction between metal atoms, between zeolite atoms and between zeolite and metal. [84] Details about the functional form of the *pcff* forcefield are included in Appendix A.

2.4.3 Estimation of Total Energy of a System using Statistical Mechanics

Statistical mechanics is the basis for the estimation of macroscopic properties of systems in equilibrium, using data from molecular simulations. There are several

references about this topic, [71,72,85] thus only essential aspects relevant to this work are discussed here.

One way of estimating macroscopic properties of systems in equilibrium from molecular simulations is by selecting representative states in a multidimensional space where the property (e.g. energy) of a traveling particle is given by $A(\vec{r}, \vec{p})$. Here $\vec{r}$ and $\vec{p}$ are the set of position and momentum vectors, respectively, which describe the state of a system. In this dissertation, the property of interest is the energy of the system, so $A(\vec{r}, \vec{p}) = E(\vec{r}, \vec{p})$. Notice that $\vec{r}$ and $\vec{p}$ are functions of time (i.e. $\vec{r} = \vec{r}(t)$ and $\vec{p} = \vec{p}(t)$). In general, the energy of a system is the mean value of sum of the individual contributions of each state during very long times of observation:

$$E = \langle E(\vec{r}, \vec{p}) \rangle = \lim_{t \to \infty} \int \left[\frac{1}{t} E(\vec{r}(t), \vec{p}(t)) \right] dt . \qquad \{ 5 \}$$

In the case of molecular dynamic simulations, the computation of the total energy of a system can be approximated by:

$$E = \langle E(\vec{r}, \vec{p}) \rangle = \sum_{i=1}^{N} \frac{1}{N} E(\vec{r}(\tau_i), \vec{p}(\tau_i)) , \qquad \{ 6 \}$$

where N is the number of iteration steps, $\vec{r}_i = \vec{r}(\tau_i)$ and $\vec{p}_i = \vec{p}(\tau_i)$; here τ_i is the time equivalent at the iteration step *i* during the simulation.

Another approach to estimate macroscopic properties is the use of the ensemble concept, as proposed by Gibbs. An ensemble is a collection of points in the multidimensional space. The theory of ensembles establishes that for a system with a defined set of properties (such as number of moles, temperature, and volume), ensembles

with the same energy states are distributed as a function of a density of probabilities (ρ). As it is expected, the probability of finding a system in each state is given by $\rho_i = \rho(\vec{r}_i, \vec{p}_i)$. Using these concepts, the total energy of a system can be calculated by:

$$E = \langle E(\vec{r}, \vec{p}) \rangle = \sum_{i=1}^{N} E(\vec{r}_i, \vec{p}_i) \rho(\vec{r}_i, \vec{p}_i) . \qquad \{ 7 \}$$

It is customary to express the density of probabilities as a quotient of a weight function of the ensemble (*w*) and a partition function (*Q*).

Partition functions are defined by the type of ensembles. In the case of the canonical ensemble, the partition function is given by

$$Q = \sum_{j=1}^{N} \exp((-E(\vec{r}_j, \vec{p}_j)/k_B T) , \qquad \{ 8 \}$$

and the weight function is given by

$$w_i = \exp(-E(\vec{r}_i, \vec{p}_i)/k_B T) . \qquad \{ 9 \}$$

Here k_B is the Plank constant and T is the temperature. Notice that in the canonical ensemble, the density of probabilities is given by the Boltzman distribution for a system at temperature T:

$$\rho_i = \frac{\exp(-E(\vec{r}_i, \vec{p}_i)/k_B T)}{\sum_{j=1}^{N} \exp(-E(\vec{r}_j, \vec{p}_j)/k_B T)} . \qquad \{ 10 \}$$

Thus the energy of a system is given by:

$$E = \langle E(\vec{r}, \vec{p}) \rangle = \sum_{i=1}^{N} \frac{E(\vec{r}_i, \vec{p}_i) \exp(-E(\vec{r}_i, \vec{p}_i)/k_B T)}{Q} . \qquad \{ 11 \}$$

When using Monte Carlo simulations for the estimation of the energy of the system, it is typical to only consider contributions of potential energy. Thus equation 11 can be reduced to:

$$E = \langle E(\vec{r}) \rangle = \sum_{i=1}^{N} \frac{E(\vec{r}_i) \exp(-E(\vec{r}_i)/k_B T)}{Q} . \qquad \{ 12 \}$$

Because it is not possible to evaluate Q using Monte Carlo techniques, the following scheme is used. [71] In a simulation in which N is the total number of points generated, the probability of finding n_i points with a state i is approximately equal to ρ_i, for $N>>1$. Because the probability of finding n_i points is basically equal to n_i / N:

$$E = \langle E(\vec{r}) \rangle = \sum_{i=1}^{N} E(\vec{r}_i) \rho(\vec{r}_i) \approx \frac{1}{N} \sum_{i=1}^{N} E(\vec{r}_i) n_i \qquad \{ 13 \}$$

Equation 13 states the basis of how the Metropolis Monte Carlo (MMC) simulations can be used to estimate the total energy of a system (E) by adding the energy contributions of each state and multiplied by the corresponding factor n_i / N. Because of the high number of iterations required for MMC simulations, the energy values of each state are usually estimated by using forcefields.

CHAPTER 3 - Literary Review

3.1 Molecular Simulations with Zeolites

There are many publications of molecular simulation studies involving zeolites, mainly related to their industrial uses. Adsorption of chemical compounds inside zeolite pores is a common denominator in many of them. The majority of these articles are on the adsorption of compounds such as hydrogen, [86] methanol, [87-89] cyclohexane, [88] methane, [90] ethane, [90] butane, [91] propane, [92] n-butane, [92] n-hexane, [92] n-pentane, [92] carbon dioxide, [93] argon, [90] nitrogen, [93] and acetronitrile. [94] Water adsorption in zeolites has been also extensively studied for mordenite, [95] Na-MAP, [96] faujasite, [97,98] and silicate. [99]

Another subject commonly studied with molecular simulations using zeolites is the diffusion of compounds inside the pores of these structures. It is no surprise that also many of these studies are related to the same compounds used in the adsorption studies, including carbon dioxide, [100] nitrogen, [100] argon, [101] methane, [101] methanol, [102] and other hydrocarbons. [103,104]

Some of the studies mentioned above include an evaluation of the proposed simulation scheme, including the selection of forcefield parameters, by making a direct comparison between estimated properties from the simulation and the ones obtained using experimental data. [87,88,91,102] Other studies evaluate the adsorption or diffusion behavior with respect zeolite characteristics such as framework type, Si/Al ratio, or the position of the acidic sites. [90,94, 105-107]

Before the research work of this dissertation, simulation studies related to the synthesis of metal nanowires in zeolites were practically nonexistent. However, in a related work by Grillo et al. [108] lattice energy minimizations were done to study the effects of different Al positions in H-mordenite framework on the location and stability of monoatomic Pt sites. Based on the lattice energy of the studied systems, the authors concluded that the stability of single Pt atoms in H-mordenite is highly influenced by the specific location of the Al atoms in the lattice.

Grillo et al. [108] also performed geometric optimizations and molecular dynamics simulations to study the effect of Pt content per mordenite cell in the size, location and structure of Pt clusters in H-mordenite. Based on the calculated energies, it was found that clusters with an optimum size of 23 atoms are confined in the 12-ring main channels, independently of the Pt content per mordenite unit cell. The simulations put remaining Pt atoms distributed in the side pockets of the zeolite structure. The structural features of the resulting clusters at the end of the molecular simulations reflected a strong metal-zeolite interaction.

3.2 Theoretical Studies on the Structure and Stability of Ultrathin Metal Nanowires

In addition to their potential use in many practical applications, ultrathin metal nanowires are widely studied because of their potential formation in never seen before atomic arrangements. These unusual structures were first predicted by Gülseren et al. in a theoretical study with Al and Pb, [109] and later studied for other materials such as Au, [110], Rh, [111] and Ni, [112] by means of molecular dynamics and geometric

optimizations using classical potentials calculations. In their work, Gülseren et al. [109] used empirical potentials developed by Ercolessi et al. [113] and Lim et al., [114] simulating an annealing process of Al and Pb nanowires. These authors found that below certain critical size (i.e. diameter) unusual non crystalline but stable and ordered structures were formed. The atomic arrangement of these structures depended on the material and wire thickness, but icosahedral packings were common. Helical and spiral structured wires with multi-atom pitches were predicted.

Wang et al. [110] studied the structures of ultrathin gold nanowires by performing geometric optimizations using a generic algorithm of molecular dynamics relaxations [115] and the potential developed by Ercolessi et al. [113] The authors found that helical structures were formed for gold nanowires at diameters less that 0.6 nm, multiwalled cylindrical nanowires were formed for diameters ranging between 1.0 to 2.2 nm, and fcc-like structures were obtained for diameters greater than 2.2 nm.

Similar results were obtained for Rh by Wang et al.. [111] These authors performed geometric optimizations of nanowires, ranging from 0.48 to 1.35 nm, using the generic algorithm of molecular dynamics relaxations of the previous study, [110,115] but energy computations were done with the empirical potential developed by Gupta et al.. [116] The nanowires obtained were formed in multishell cylinder like structures consisting of helical rows of atoms. Among the structures obtained, there were trigonal, tetragonal, centered pentagonal, and centered hexagonal packings.

Peng et al. [112] used molecular dynamic simulations with the embedded atom method (EAM) potential [117] to study the structural stability of Ni nanowires. The authors used several conditions for simulations, including annealing and submission to

linear strand at the center formation. In this work, various configurations of ultrathin Ni nanowires were constructed with predetermined configurations and then exposed to static relaxation. Depending on the starting geometry, some nanowires keep their original form with slight changes in lengths and radii and others evolved to different structures. As with the other studies discussed before, many of the stable nanowires resulted in helical multi-shell structures.

Similar studies on the stability of metal nanowires using Density Functional Theory (DFT) geometric minimizations have been done for Al, Cu, Ag, Au, Ni, Pd, and Pt. Some of them are discussed in the following paragraphs.

The structural stability of Al nanowires was studied by Makita et al. [118] using DFT calculations with periodic boundary nanowire models. For unit cells of 8.361Å × 8.361Å × L, structures were not stable against deformation because of the interaction with other nanowires in the neighboring cells; however, vibrational modes of deformation showed stability for the 14.817 Å × 14.817 Å × L. The estimated energy per atom rose considerably when the radius of the nanowire got shorter. Stability with respect to elastic deformation increased as the radius became larger. On the other hand, Zheng et al. [116] studied the stability and electronic structure of single monoatomic Al wires with (DFT) and found two stable configurations that follow a zigzag pattern with angles of 140° and 60°.

Zarechnaya et al. [120] studied the binding and electronic properties of monoatomic nanowires, dimers and bulk structures of Cu, Ag, Au, Ni, Pd, and Pt using DFT geometric optimizations. The authors found that the formation of atomic chains is

not possible for all the elements studied. Results showed that Pt and Au are the most likely elements to form monoatomic nanowires.

The research work discussed above was oriented mainly to find stable structures by means of geometric optimizations; some of them using a combination of molecular dynamics and energy minimization schemes with potentials, others using energy minimizations with DFT. However, as discussed in the previous chapter, geometric optimized structures are representations of systems at 0 K, that is, thermal effect is not considered in the overall stability of these atomic arrangements. Some of the works on metal nanowires that deal with this issue are discussed in the following paragraphs.

The thermal stability of Ni ultrathin nanowires has been studied by Wen et al. [121] using molecular dynamics simulations. These simulations suggest that the temperature at which deformation (or melting) of the metal nanowires occurs is much lower than the melting temperature of bulk materials. It was also found that there is an inverse linear relationship between the melting temperature and the diameter of Ni nanowires. For nanowires where no external strain was applied, the structures collapsed to spherical clusters at the melting temperature.

Koh et al. [122] studied the behavior of infinitely long cylindrical platinum nanowires with a 1.4 nm diameter at different uniaxial tensile strains along the (001) axis, using molecular dynamics simulations with an empirical potential expression developed by Cleri et al. [123] and parameterized by Sutton et al.. [124] In this work, Pt nanowires preserved crystal order and stability at the lower temperature (50K) and strain rate (0.04% ps^{-1}). Partial crystal deformation was observed at 0.4% ps^{-1} and fully amorphous

deformation occurred at 4.0 ps^{-1}. Amorphous melting of the crystalline structure took place at 300K for small tensile strains.

Chapter 4 - Si/Al and Metal Loading Effects on the Synthesis of Ni Nanowires in CAN & MOR

4.1 Introduction

As mentioned in section 3.1, Grillo et al. [108] published a molecular simulation study on the stability of metal particles inside zeolites. In this work, the authors pointed out that the positions of Al atoms in the zeolite framework have a strong influence on the stability of monoatomic Pt particles at different locations. When two Al atoms where placed on the T1-T4, T3-T4, or T2-T4 sites of H-mordenite (see Figure 4.1), relative lattice energies of -293.3, -294.79, and -277.88 kcal/mol where obtained, respectively, favoring a Pt location inside the side pockets. On the other hand, when the Al atoms where placed on the T1-T3, T1-T2, or T3-T2 sites of H-mordenite, relative lattice energies of -274.73, -260.31, and -256.25 kcal/mol where obtained, respectively, favoring a Pt location inside the main channel pores. Taking into account the T3 and T4 sites are energetically favored to host Al atoms (which is ultimately reflected on expected percent of Al with respect to each tetrahedral site of mordenite), the authors concluded that the side pockets are favored energetically to host Pt atoms in zeolite mordenite, which is the zeolite with the MOR framework and low values of Si/Al.

For the synthesis of ultrathin nanowires through templated synthesis it is desired that most of the guest metal particles remain in the main pores channels of the zeolite. The reported effect of the location of Al in the positioning of guest metal atoms is thus very relevant. The molecular simulation studies presented here address the influence of

the aluminum sites, as well as the zeolite framework type and metal loading, in the positioning of guest metal atoms at the end of the synthesis process.

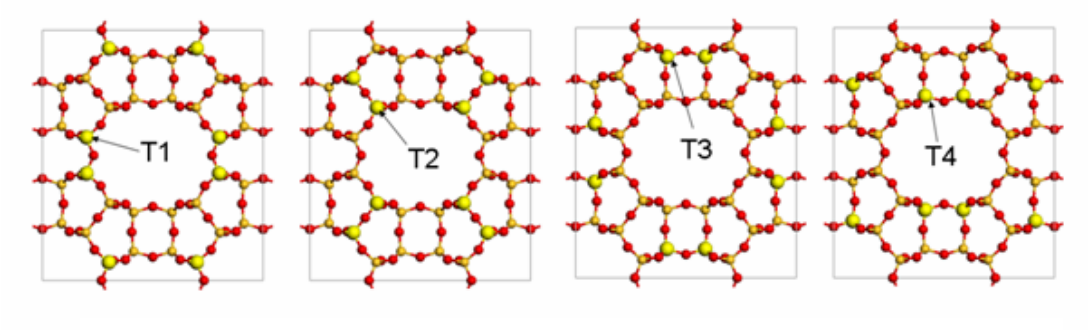

Figure 4.1 - Position of T sites in MOR unit cell (*identified by bigger spheres*)

For the actual synthesis process of zeolites, the Si/Al and not the location of Al atoms can be controlled. Thus, theoretical studies can be accurately performed only with zeolites where the positioning of the Al atoms can be uniquely identified. These are the cases of the two one dimensional pore frameworks selected for simulations performed in this chapter: cancrinite (CAN) and mordenite (MOR) type zeolites. Based on this, we selected the CAN framework with Si/Al = 1 and Si/Al = ∞, and the MOR framework with Si/Al = 5 and Si/Al = ∞ as study cases. In addition to the above mentioned characteristics, MOR was selected because zeolites with this framework (i.e. mordenite) are commercially available at different Si/Al ratios. On the other hand, the CAN framework was selected because it has a smaller pore diameter than MOR; also CAN-type zeolites (i.e. cancrinite and the Exxon Corporate Research Five (ECR-5)) can be synthesized at the minimum Si/Al ratio possible (i.e. one).

The main pore channels of CAN-type zeolites have a diameter of 5.9 Å, measured between two opposed oxygen atoms (see Figure 4.2). The rings that form these main pore channels have 12 oxygen atoms. These main pore channels are surrounded by side pockets with rings formed by four and six oxygen atoms. The interconnecting rings between the main pore channels and the side pockets of the CAN framework have an effective diameter of approximately 1.5 Å.

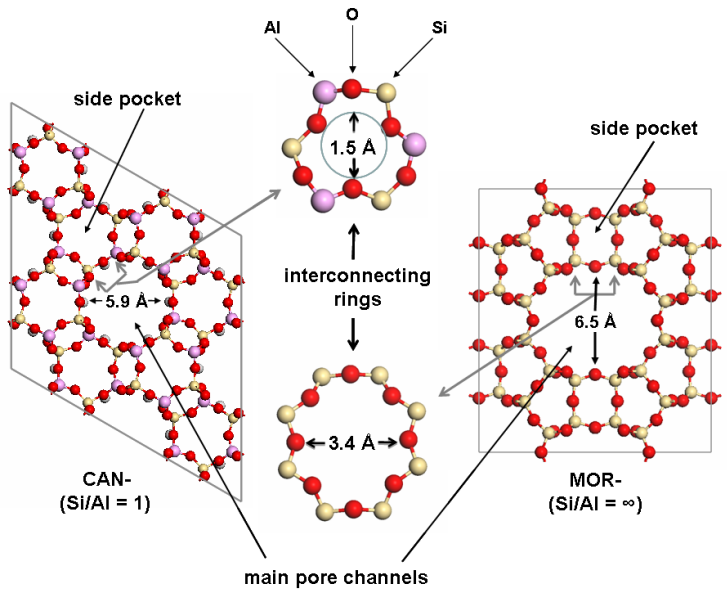

Figure 4.2 - Cancrinite (CAN) and mordenite (MOR) frameworks

In the case of the MOR framework, the smallest distance between two opposite oxygen atoms in the main pore channel is 6.5 Å. These channels have rings of 12 oxygen atoms and are surrounded by different side pockets with windows that have between four and eight oxygen atoms. For the larger windows, the minimum distance between two opposed oxygen atoms is ~ 3.4 Å.

Ni nanowires have outstanding magnetic properties such as high perpendicular anisotropy and inversely proportional coercivity with respect to diameter. [125]

4.2 Simulation Methodology

Molecular simulations and geometric optimizations described in the following paragraphs were performed using the Sorption and Forcite modules of Material Studio Software™, Version 4.0 (Accelrys, Inc.). Wherever the Metropolis Monte Carlo (MMC) scheme was performed, the canonical ensemble was used with 2×10^6 equilibration steps, 1×10^7 processing steps, and a cut off ratio of 18.5Å. For these MMC simulations, the temperature was set to 298 K.

4.2.1 Energy computations

The *pcff* forcefield introduced in Chapter 2 was used for the energy computations required in both the geometric optimizations and MMC simulations presented here. *Pcff* is well known and extensively used forcefield developed by Sun et al., and it is based on the *cff* forcefield. [82,83] The parameterization of the *pcff* for the metal-metal interactions is based on the 9-6 form of the Lennard-Jones potential and was obtained by fitting parameters to crystal structures and elastic constants of the selected metals. [84]

4.2.2 Supercell definition and positioning of the Al atoms in CAN and MOR

The molecular simulations presented here were performed using the CAN-type

zeolites with Si/Al = ∞ and Si/Al = 1, and the MOR-type zeolites with Si/Al = ∞ and Si/Al = 5. For CAN-type zeolites, a supercell composed of 2 x 2 x 16 basic unit cells (containing 2304 atoms) was used. In the case of MOR-type zeolites, the supercell used was composed of 1 x 1 x 16 basic unit cells (also containing 2304 atoms).

The relative position of the atoms in the frameworks used was fixed during simulation processes and determined previously from crystallographic data. The positioning of the Al atoms for CAN framework with Si/Al = 1 is easily obtained with the Löwenstein rule, which states that two Al atoms cannot be connected to the same O atom in the zeolite structure, due to energetic stability considerations.

For the MOR-type zeolite with Si/Al = 5, the positioning of the eight Al atoms per unit cell was selected using a similar criteria to the one used by Demuth et al.; [126] the Al atoms were preferentially positioned at the T3 sites and secondly at the T4 sites (shown in Figure 4.1), which are the preferred T-sites for Al atoms in zeolite mordenite. The empirical Löwenstein rule was also applied, which states that the presence of two Al atoms bonded to the same oxygen atom is highly unlikely. There are eight T3 sites in the MOR framework basic unit cell; the Löwenstein rule only permits the positioning of a maximum of four Al atoms in them. The same is true for the T4 sites, thus the eight Al atoms can be positioned in the T3 and T4, occupying completely the available positions for those two sites in the basic unit cell of MOR-type zeolite. To establish the position of the charge-balancing protons in the alumina rich CAN and MOR-type zeolites, geometric optimizations were done for the several configurations selecting the ones that resulted in a lower total energy.

4.2.3 One Ni atom simulations for CAN and MOR-type zeolites

In order to study the interaction between Ni and the two different zeolite frameworks, MMC simulations were performed with a loading of one Ni atom. The purpose was to establish the conditions that promote the displacement of Ni within the one-dimensional main pores channels by avoiding diffusion to the side pockets. In these simulations, the path of a single Ni atom through the framework was used to generate frequency plots. The resulting plots help visualize the effect of the zeolite framework structure and composition (Si/Al) over the Ni preferred positions, when considering only the interaction between the guest metal and zeolite atoms.

4.2.4 Energy minimizations for one Ni atom inside CAN and MOR-type zeolites

Geometric optimizations were done with one Ni atom to find local energy minima for the positioning of Ni in the main pore channels and in the side pockets of CAN and MOR-type zeolites at the different Si/Al. For these minimizations, the relative position of the zeolite atoms was fixed. To find the local minima, the Ni atom was placed initially at both the geometrical center of each structure and near the positions obtained from the ten snapshots with the lowest potential energy reported by the one Ni atom MMC simulations. As mentioned before, the MMC simulations performed 1×10^7 processing steps that served to screen the conformational space of unit cells of the zeolites. The minimizations were done using the conjugate gradient algorithm and conversion was reached at tolerances of 2.0×10^{-5} kcal/mol for energy, 1.0×10^{-3} kcal/(mol Å) for force, and 1.0×10^{-5} Å for displacement.

4.2.5 MMC simulations for zeolite frameworks at different Si/Al and metal loadings

Evaluation of the spatial distribution of Ni atoms within the CAN and MOR frameworks with different Si/Al was done using MMC simulations at Ni loadings equivalent to 5, 10, 15 and 19% w/w. These simulations were done to obtain the relative position of Ni atoms at the most stable energetic conditions (minimal energy configurations). The simulations were conducted in order to determine the conditions that promote the formation of one dimensional nanostructures inside the main pore channels.

4.3 Results and Discussion

Figure 4.3 presents the results of one Ni atom simulations for CAN-type zeolites with Si/Al = ∞ and Si/Al = 1. Figure 4.4 presents the equivalent results for MOR-type zeolites with Si/Al = ∞ and Si/Al = 5. In these figures the trace of the center of the Ni atom is plotted for the movements generated by the MMC algorithm. In repeated MMC simulations of CAN-type zeolite with Si/Al = 1 and loadings of one atom, the side pockets of the zeolite were not a preferred location for Ni. In MMC simulations of CAN-type zeolite with Si/Al = ∞ and one Ni atom, Ni was positioned in either the side pockets or the main pore channels. We observed an interrupted path generated by the algorithm for Ni in this zeolite framework, i.e., the Ni atom initially positioned at the main pore channels did not pass through the interconnecting ring to the side pockets and vice versa. On the other hand, one Ni atom simulations in MOR-type zeolites (Si/Al = ∞ and

Si/Al = 5) suggest that this behavior is different; the Ni atom passed through the interconnecting ring from the main pore channel to the side pockets and vice versa.

These differences can be explained by the diameter of the larger interconnecting rings of these two frameworks, which is ~ 1.5 Å for CAN and ~ 3.4 Å for MOR (see Figure 4.2). With a van der Waals atom diameter of 3.26 Å, Ni atoms are hindered to pass through the CAN-type zeolite interconnecting rings. In this respect, CAN-type zeolites results in a better alternative than MOR-type zeolites for the templated synthesis process of Ni nanowires.

The behavior of Ni in CAN framework and its absence from the side pockets for the zeolite with Si/Al = 1 suggests that these are not an energetically favorable sites for the guest metal atoms. This was confirmed by energy minimizations of one Ni atom in the side pockets and in the main pore channels for the CAN-type zeolites with Si/Al = 1 and Si/Al = ∞. The results of these energy minimizations are presented in Figure 4.5a and Table 4.1. The values of ΔE correspond to the difference between the energy of the described system (zeolite framework and Ni atom) and the energy of the zeolite framework alone, as the potential energy reported by the forcefield for a single Ni atom with no influence of the zeolite framework is a referential one, and its value is zero.

For the specific case of one Ni atom in the side pocket of the CAN-type zeolite (Si/Al = 1), the ΔE is positive suggesting that the positioning of Ni in this place is not favored at these conditions.

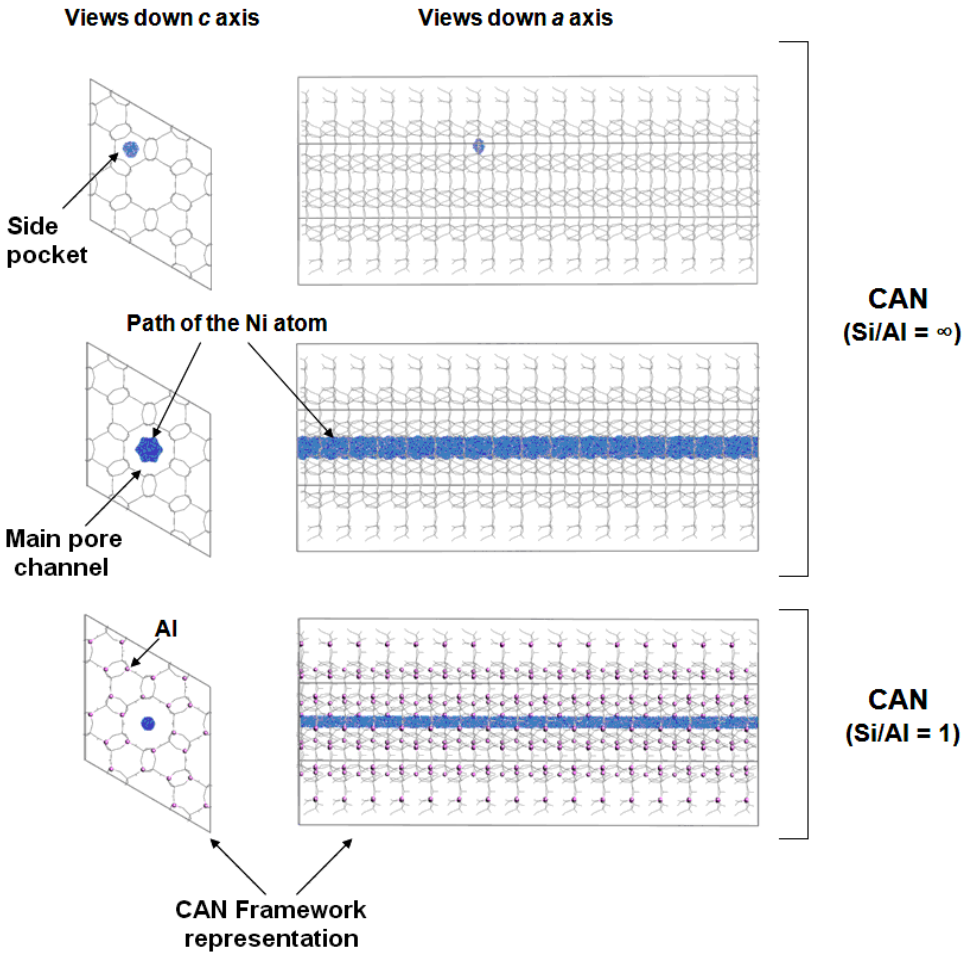

Figure 4.3 - Distribution plots for MMC simulations of one Ni atom in the CAN framework

The plots of the MMC simulations in Figure 4.4 reflects that for the MOR framework with Si/Al = ∞, the positioning of Ni in the side pockets is favored; meanwhile the positioning of Ni in the main pore channel is more significant for the MOR-type zeolite with Si/Al = 5. These results are consistent with the energy minimizations of one Ni atom inside the side pockets and the main pore channels of MOR-type zeolites with Si/Al = 1 and Si/Al = 5 (see Figure 4.5b and Table 4.2).

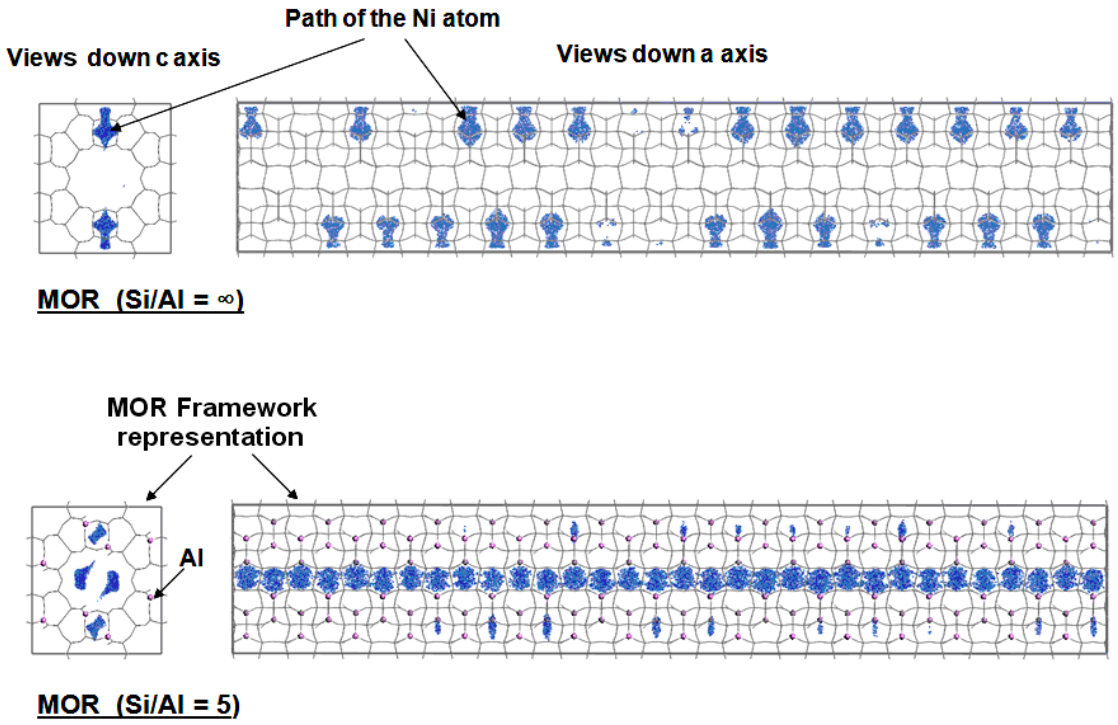

Figure 4.4 - Distribution plots for MMC simulations of one Ni atom in the MOR framework

As observed in Figures 4.3 and 4.4, the presence of Al in the zeolite structure promotes a separation of the Ni neutral atom from the wall surfaces of the zeolite structure. This behavior suggests that van der Waals repulsion forces between Ni and the oxygen atoms bonded to Al atoms are stronger than the forces between Ni and the oxygen atoms bonded to Si atoms.

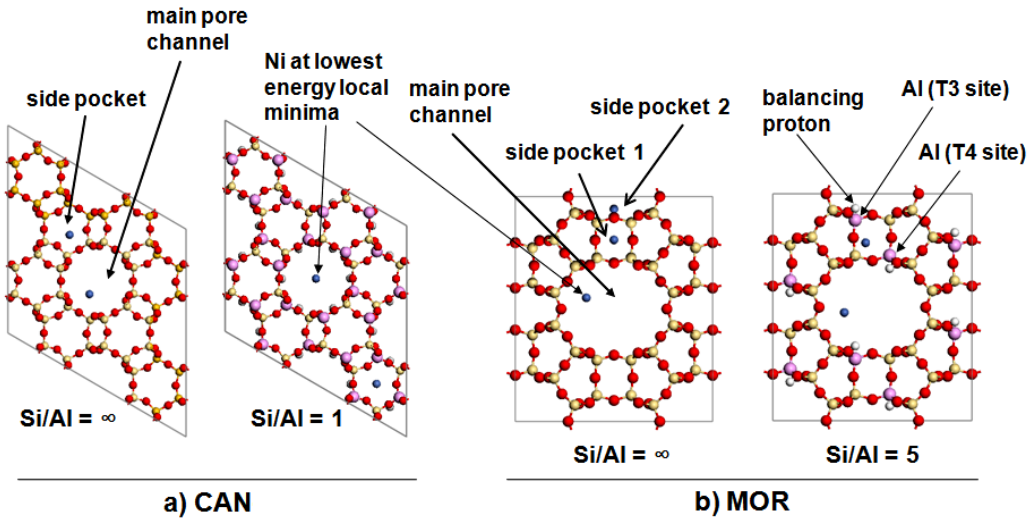

Figure 4.5 - Positions after local energy minimizations of one Ni atom in the CAN and MOR frameworks

Table 4.1 - Energy of one Ni atom in CAN framework pores (in kcal/mol)

System	Total Energy	Δ Energy(*)
CAN - type zeolite (Si/Al = ∞)	-28 009.9	0.0
+ Ni main channel	-28 017.2	-7.3
+ Ni side pocket	-28 020.3	-10.4
CAN - type zeolite (S/Al = 1)	-90 155.3	0.0
+ Ni main channel	-90 158.3	-3.0
+ Ni side pocket	-90 153.0	2.3

(*) ΔEnergy = Energy of system considered minus Energy of CAN-type zeolite at the corresponding Si/Al

Table 4.2 - Energy of one Ni atom in MOR framework pores (in kcal/mol)

System	Total Energy	Δ Energy(*)
MOR-type zeolite (Si/Al = ∞)	-43 011.3	0.0
+ Ni main channel	-43 019.2	-7.9
+ Ni side pocket 1	-43 020.8	-9.5
+ Ni side pocket 2	-43 021.3	-10.0
MOR-type zeolite (Si/Al = 5)	-52 891.8	0.0
+ Ni main channel	-52 898.8	-7.0
+ Ni side pocket 1	-52 897.7	-5.9
+ Ni side pocket 2	--------	----

(*) ΔEnergy = Energy of system considered minus Energy of MOR-type zeolite at the corresponding Si/Al

Figure 4.6 shows the views down the *c* axis of MMC simulations results for CAN-type zeolites with Si/Al = ∞ and Si/Al = 1 at different Ni loadings. These views present the minimum energy configurations obtained with the MMC algorithm. In these schematics it is observed that Ni is almost absent from the side pockets of the CAN-type zeolite with Si/Al = 1 at all loadings, meanwhile guest metal atoms are consistently present in the side pockets of the CAN-type zeolite with Si/Al = ∞ at all loadings. For the CAN framework with Si/Al = 1, only at the highest metal loading studied (19% w/w) Ni atoms were observed in the side pockets. Positioning of the Ni atoms in the main pore channel follow a similar trend to that observed in the one Ni atom simulations; the Ni atoms for CAN-type zeolite with Si/Al = 1 are more distanced from the zeolite walls than the corresponding Ni atoms in CAN-type zeolite with Si/Al = ∞, resulting in more compact Ni agglomerates. The consistency of this behavior in simulations at different Ni loadings supports our prior observation that the presence of Al atoms promotes the repulsion of Ni atoms from the walls of the zeolite framework.

Figure 4.7 presents the results for MMC simulations of MOR-type zeolites with Si/Al = 5 and Si/Al = ∞ at different Ni loadings. Here the pattern observed is similar to the one showed by the MMC simulations for the CAN framework; the simulations of MOR-type zeolite with the lower Si/Al strongly favors the positioning of the metal atoms inside the main pore channels and higher Si/Al promotes the displacement of Ni into the side pockets. This behavior is consistent to the results observed in the one Ni atom MMC. However, the effect of Ni concentration on the positioning of the guest metal atoms is different in MOR-type zeolite than in CAN-type zeolite with Si/Al = ∞. For the MOR framework, loadings higher than 5% (w/w) seems to favor a displacement of the Ni atoms from the side pockets to the main pore channel. This behavior seems to be related to the attraction forces that exist between the Ni metal atoms and the availability of a greater space in the main pore channels to accommodate them. In the case of CAN-type zeolite (Si/Al = ∞) as the Ni loading is increased, an increase in the number of guest metal atoms of both the main pore channels and the side pockets is observed. The latter behavior can be attributed by the hindrance of Ni to pass through the interconnecting rings between the side pockets and the main pore channels after the aleatory positioning of metal atoms in the loading steps of the MMC algorithm.

Figure 4.8 shows the Ni positioning results of MMC simulations in views down the *a* axis along the supercells of MOR-type zeolites with Si/Al = ∞ and Si/Al = 5 and at Ni loadings of 10% w/w. A view of MOR-type zeolite (Si/Al = 5) with 19% w/w Ni loading is also included. In the MCC simulations of MOR-type zeolite at lower Ni loadings, the formation of Ni clusters was observed. At higher Ni loadings with

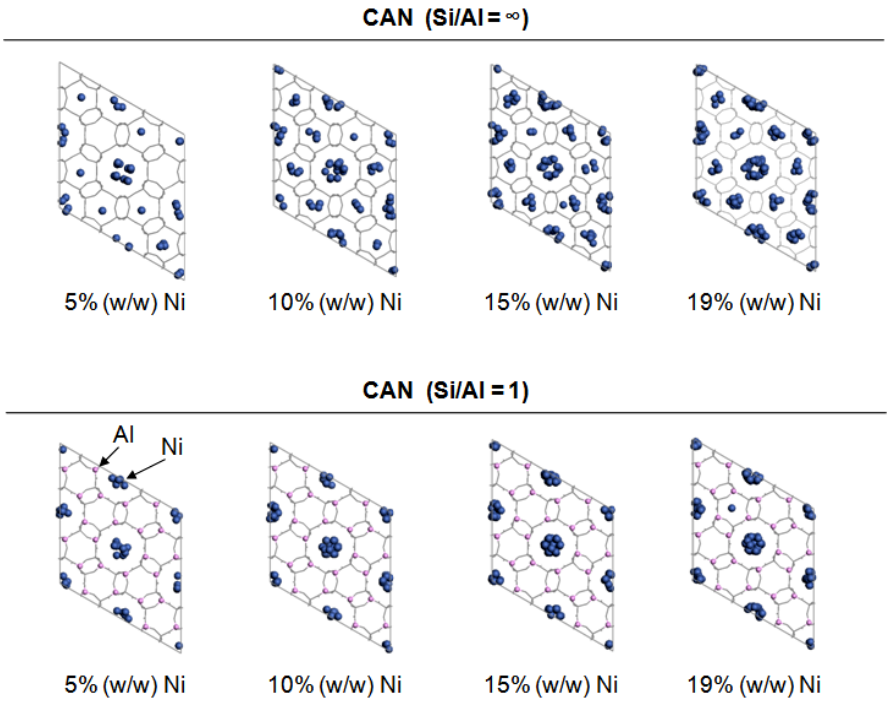

Figure 4.6 - Distribution plots for MMC simulations of Ni in CAN at different Si/Al and metal loadings (views down the *c* axis)

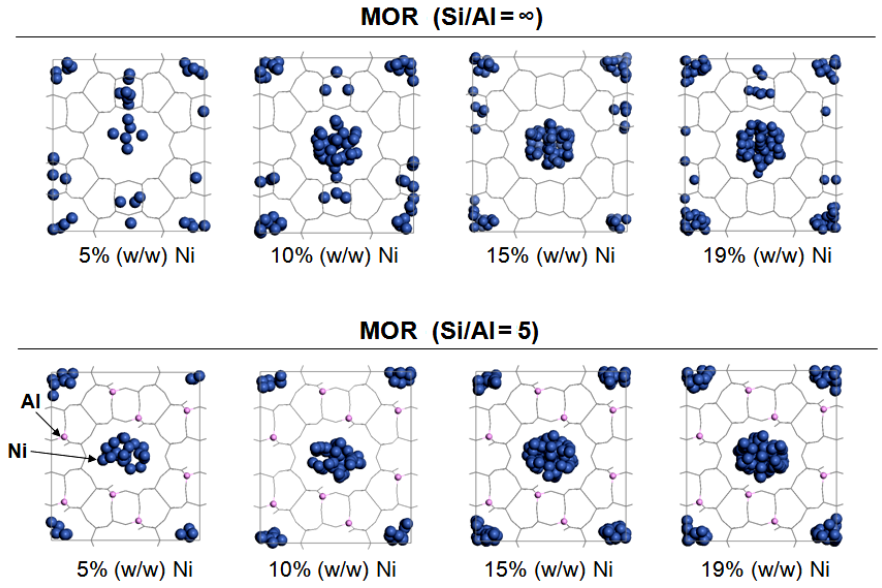

Figure 4.7 - Distribution plots for MMC simulations of Ni in MOR at different Si/Al and metal loadings (views down the *c* axis)

Si/Al = 5, the observed size of the clusters at the main pore channels was generally greater than for MOR-type zeolite at Si/Al = ∞. As the metal concentration increased, the observed Ni agglomerates in MOR framework (Si/Al = 5) elongated as observed in Figure 4.8c. These patterns were also observed for the MMC simulations of the CAN framework. These results suggest that low Si/Al and high metal loadings promote the formation of metal nanowires in the MOR framework.

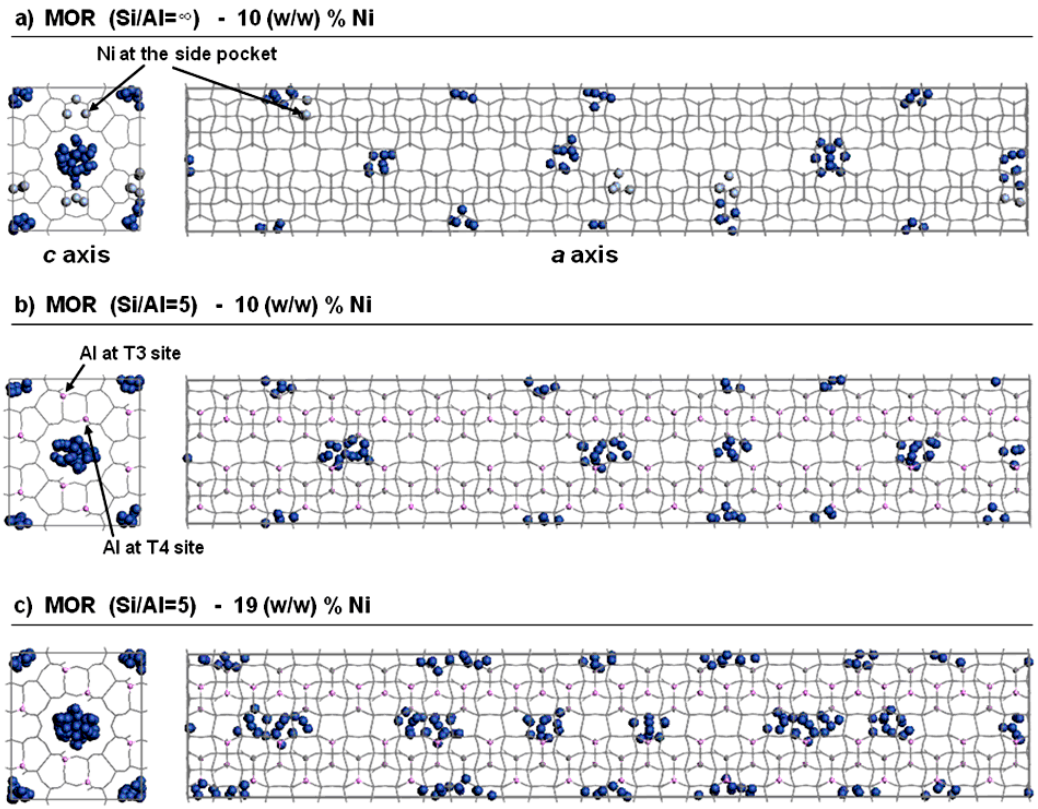

Figure 4.8 - Selected MCC simulations results of Pt in MOR framework with views down the c and *a* axis *(lighter spheres represent Ni atoms in the side pockets)*

4.4 Conclusions

Our results illustrate the importance of the zeolite framework, Si/Al, and metal loading in promoting the synthesis of metal nanowires using zeolite structures. For CAN and MOR frameworks, a low Si/Al favored energetically the positioning of Ni atoms inside the main pore channels. This suggests that lower Si/Al can reduce the displacement of metal guest atoms from the main channels to the side pockets, improving the potential of such frameworks to be used in the templated synthesis of metal nanowires. In frameworks like CAN, the small dimensions of the interconnecting rings prevent the migration of Ni and other metal atoms from the main pore channels to the side pockets. This fact can be useful during the templated synthesis of metal nanowires if adequate size precursor molecules are used during impregnation, to place the metals atoms initially inside the main pore channels of the zeolite framework.

In the case of the MOR framework, the effect of lower Si/Al acquire more relevance for the templated synthesis process because the greater size of the interconnecting rings allows the displacement of the metal atoms between the main pore channels and the side pockets. This can have a detrimental effect for the synthesis of metal nanowires; however, based on the results obtained in the MMC simulations presented here, the migration of metal atoms from the main pore channel to the side pockets can be highly reduced if low Si/Al and high metal loadings are used.

In general, higher Ni loadings were necessary for the formation of elongated structures while smaller rounded clusters were favored at lower Ni loadings. In the case of MOR-type zeolites, the combination of high Ni loadings and low Si/Al ratios promote

the formation of elongated structures and therefore seem to be the suitable combination for the synthesis of Ni nanowires.

When comparing the results obtained with CAN and MOR-type zeolites, the CAN frameworks seem to be a better option than MOR frameworks for the synthesis of metal nanowires. However there are several practical considerations that must be taken into consideration when evaluating these frameworks for their use as templates. For example, the zeolite cancrinite (which has a CAN framework with Si/Al = 1) presents several problems related to the commercial availability of the zeolite and the removal of the template compounds used to synthesize it; meanwhile, zeolites with the MOR framework such as mordenite are easier to manage and are available commercially.

The results presented here illustrate the influence of the structure of the zeolite in the minimum energy locations of the Ni atoms inside the pores. This suggests that there is a set of optimum zeolite framework characteristics for the formation of nanowires.

Chapter 5 - Effect of Temperature, Si/Al, and Metal Loading on the Positioning of Pt Atoms in MOR-type Zeolites

5.1 Introduction

The use of traditional synthesis methods, such as wet impregnation of precursors and reduction of these compounds at high temperatures, results in the formation of small clusters inside the zeolite templates. [61,62] However, there is evidence that elongated clusters of Pt could be formed inside the pores of mordenite with these methods. [127]

Through the simulations presented in Chapter 4, it was found that under certain conditions the displacement of metal atoms is permitted through the interconnecting rings of the MOR framework allowing the migration of the metal atoms to the side pockets (see Figure 5.1). This fact can have a detrimental effect on the synthesis of metal nanowires and could partially explain why the formation of clusters and elongated clusters is favored instead of larger one dimensional nanowires. Results discussed in Chapter 4 also revealed that the positioning of guest metal atoms in MOR can be influenced by the Si/Al of the zeolite and the local concentration of the guest metal atoms. However, other factors can affect the behavior of metal atoms inside zeolites with accessible side pockets. One of them is temperature, which probably has a direct influence on the diffusion of these metal atoms inside the zeolite framework.

Another factor that can affect the displacement of metal atoms the nature of the metal used. The size of these atoms and the interaction forces between them and those in the zeolite framework is also another important variable to consider.

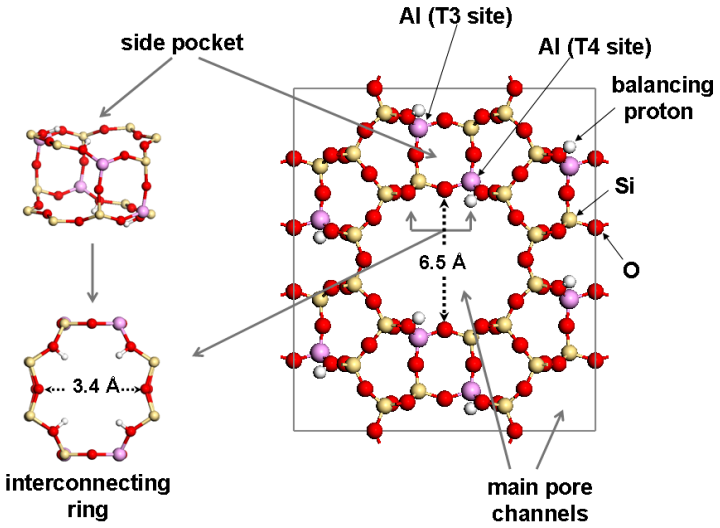

Figure 5.1 - Location of interconnecting rings and Al atoms in the MOR framework (Si/Al = 5)

In the work presented in this Chapter, the effect of temperature and the use of Pt is considered in combination with other factors already studied. Pt is a metal used in electronic circuits and has excellent catalytic properties. Geometric optimizations, Metropolis Monte Carlo, and molecular dynamics simulations were performed to study the effect of temperature, in combination with Si/Al and metal loading, on the positioning of Pt metal atoms in the MOR and how it changes with time. While both Ni and Pt have similar characteristics as they are transition metals of the same group, Pt is a larger atom with greater atomic mass so a comparison with analogous studies in Chapter 4 is included.

5.2 Simulation Methodology

The geometric optimizations and molecular simulations described here were done with the Sorption and Forcite modules of Material Studio Software™ (Accelrys, Inc.), Version 4.0 and 5.0, respectively. Molecular simulations were done using the Metropolis Monte Carlo (MMC) and molecular simulation (MD) schemes under the canonical ensemble. The energy computations were done using the *pcff* forcefield developed by Sun et al.. (82,83)

Charges of atoms were forcefield assigned and interactions between charge groups were calculated using a group-based sum; other electrostatic interactions were calculated using Ewald summation. The maximum displacement of the MMC simulations was set to 1 Å. The energy values were calculated using a cut of ratio of 18.5 Å, with a cubic spline truncation set to 1.0 Å and a buffer set to 0.5 Å.

5.2.1 Supercell definition and the positioning of the Al atoms in MOR

The simulations studies described here were done using the MOR framework with Si/Al = ∞ and Si/Al = 5. The MOR supercell was constructed using an arrangement of 1 x 1 x 16 basic unit cells (consisting of 2304 atoms). The relative position of the atoms in the MOR framework, was fixed during all simulation processes (i.e. rigid zeolite framework), and previously determined from crystallographic data. In the case of MOR with Si/Al = 5, the positioning of the eight Al atoms per unit cell was selected using a similar criteria to the one used by Demuth et al.; [126] the Al atoms were preferentially positioned at the T3 sites and secondly at the T4 sites (shown in Figure 5.1), which are

the preferred T-sites for Al atoms in zeolite mordenite. Also, the empirical Löwenstein rule was applied, which states that two Al atoms cannot be connected to the same O atom in the zeolite structure, due to energetic stability considerations. Additional details of the criteria used for the positioning of Al in MOR (Si/Al = 5) are described in Chapter 4.

To establish the position of the charge-balancing protons in MOR (Si/Al = 5), geometric optimizations (with fixed framework atoms) were done for the charge balancing protons considering several configurations. Each configuration was constructed by assigning a proton to a specific oxygen atom of the Al tetrahedral in the T3 and T4 sites. The final position of the protons was established by selecting the optimized configuration with the lowest potential energy.

5.2.2 MMC One Pt atom simulations

MMC simulations were performed with a loading of one Pt atom to study the interaction between Pt as guest metal and the zeolite framework atoms with different Si/Al ratios (∞ and 5), at temperatures of 298 and 623 K. In these simulations, the path of the Pt atom was used to generate distribution plots that help to visualize the preferred positions of the Pt atoms in MOR as a function of the above mentioned conditions.

5.2.3 Energy minimizations for one Pt atom inside MOR

Geometric optimizations were done with one guest metal atom to find the positioning of the local energy minima of Pt in the main pore channels and side pockets of the MOR framework at different Si/Al. For these geometric optimizations, the relative position of the zeolite atoms was fixed. To find the local minima, the Pt atom was placed

initially at both the geometrical center of framework structure and near the positions with the lowest energy obtained from MMC simulations described in section 5.2.2. The geometric minimizations were done using the conjugate gradient algorithm and conversion was reached at tolerances of 2.0×10^{-5} kcal/mol for energy, 1.0×10^{-3} kcal/(mol Å) for force, and 1.0×10^{-5} Å for displacement (see details in section 4.2.4).

5.2.4 MMC Simulations at different temperatures, Si/Al and Pt loadings

Evaluation of the spatial distribution of Pt atoms within the MOR framework at 298 K and 623 K, and at the Si/Al ratios mentioned above, was done using MMC simulations at Pt loadings equivalent to 1, 2.5, and 5% (mol/mol). These simulations were done to obtain the relative position of Pt atoms at the most stable energetic conditions using the frequency plots as explained in section 5.2.2. For these simulations, 6×10^6 equilibration steps and 2×10^7 processing steps were used.

5.2.5 MD Simulations for MOR at different temperatures and Si/Al

In order to study the dynamic behavior of Pt atoms inside MOR at the different Si/Al and temperatures mentioned above, molecular simulations were performed with a loading of 14 guest metal atoms positioned in a straight line at the center of the main pore channel. The Pt atoms were initially distributed at a distance of 11.442 Å from the extremes of the MOR supercell and 7.524 Å between two consecutive atoms of the guest metal. The time for each iteration step was fixed to 0.1 fs and the total simulation time was set to 1000 ps, resulting in 1×10^7 simulation steps. The temperature was fixed using the NOSE thermostat algorithm and the initial velocities were assigned randomly.

5.3 Results and Discussion

5.3.1 MMC Simulations and geometric optimizations

The frequency plots from MMC simulations with one Pt atom in MOR are presented in Figures 5.2a to 5.2d. At both temperatures considered, when Si/Al = ∞ the path of the Pt atom suggests that the presence of this metal in the side pockets of MOR is favored. On the other hand, when Si/Al = 5 the preferred position of the Pt atom is shifted from the side pockets to the main pore channels of the structure. This is consistent with previous results obtained for Ni in MOR.

Comparison of the results obtained at room temperature and at 623 K suggests that there is an energy barrier on MOR that reduces the ability of Pt to pass through the interconnecting rings between the side pockets and the main pore channels. This energetic barrier can be due to the fact that the diameter of the interconnecting rings is about the same magnitude of the van der Waals diameter of the Pt atom (3.5Å). At 623 K, the acceptance of the random walk through the interconnecting ring by the MMC scheme is greater than the observed at 298 K, making possible for the Pt atom to visit more frequently the less energetically favored places.

Geometric minimization results for one Pt atom inside the MOR framework are presented in Figure 5.3 and Table 5.1. These local minimum energy positions were obtained indistinctively of varied nearby initial positions of the Pt atoms. The values of the total energy corresponds to the energy estimated using the *pcff* forcefield for the system described in column 1, which consists of the supercell of the MOR zeolite or this supercell plus one Pt atom at the local energy minimum. The values of ΔE correspond to

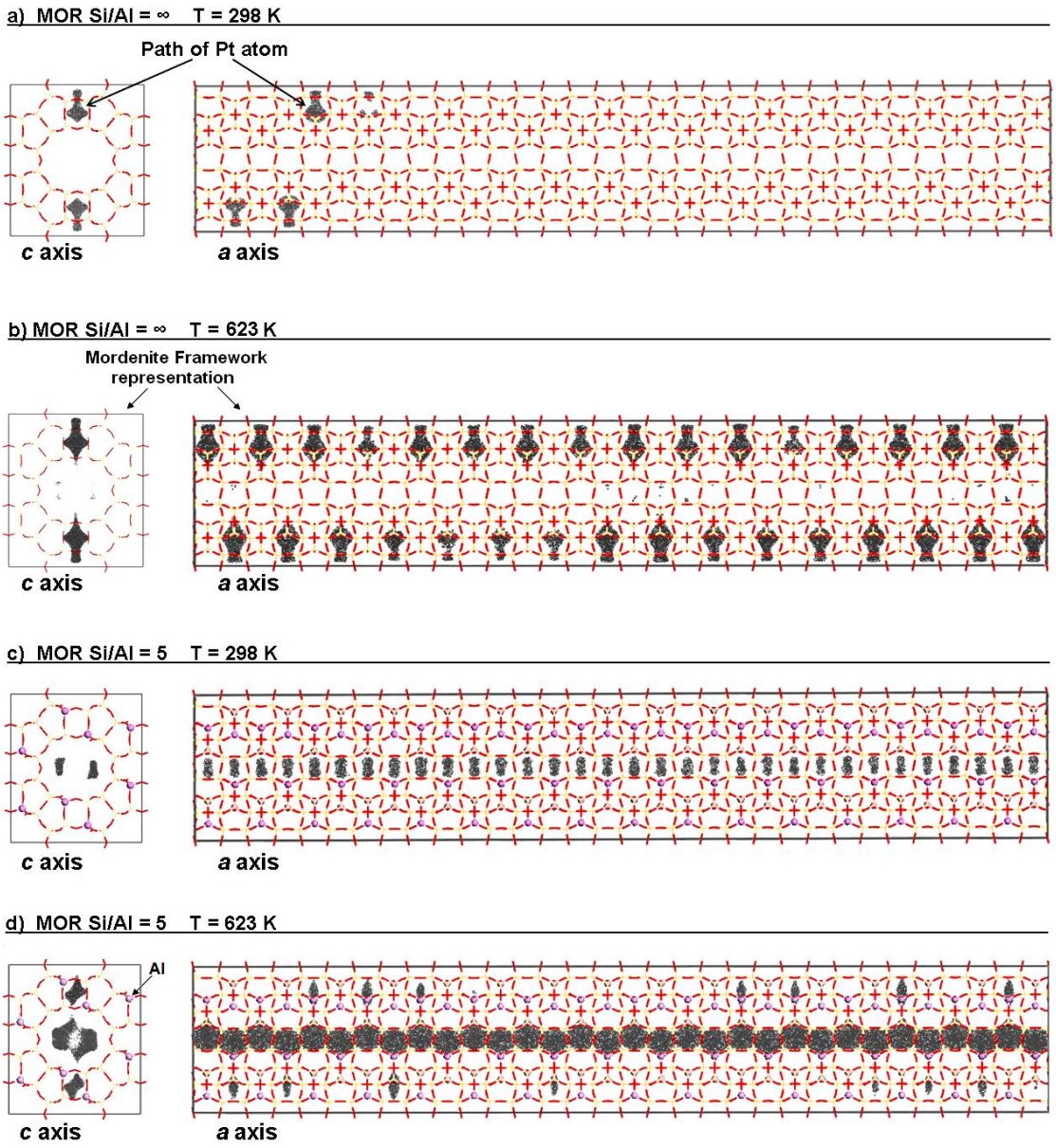

Figure 5.2 - Distribution plots for MMC simulations of one Pt atom in the MOR framework

the difference between the energy of the described system (zeolite framework and Pt atom) and the energy of the zeolite framework alone, as the potential energy reported by the forcefield for a single Pt atom with no influence of the zeolite framework is a referential one, and its value is zero. ΔE values for each of the local minima obtained at

the main pore channel and the side pockets of the framework are consistent with the results obtained for the MMC simulations with one Pt atom. For MOR with Si/Al = ∞, ΔE is lower at each of the two local minima found in the side pockets than ΔE at the local minima of the found at the main pore channel. These lower energy values indicate that for MOR with Si/Al = ∞, the more stable sites for Pt are in the side pockets of the structure. For the case of MOR with Si/Al = 5, the most stable energetic position is shifted to the main pore channels of MOR. Only one additional position for the local minima was found at the side pockets of the framework which was slightly less stable than the position in the main channel.

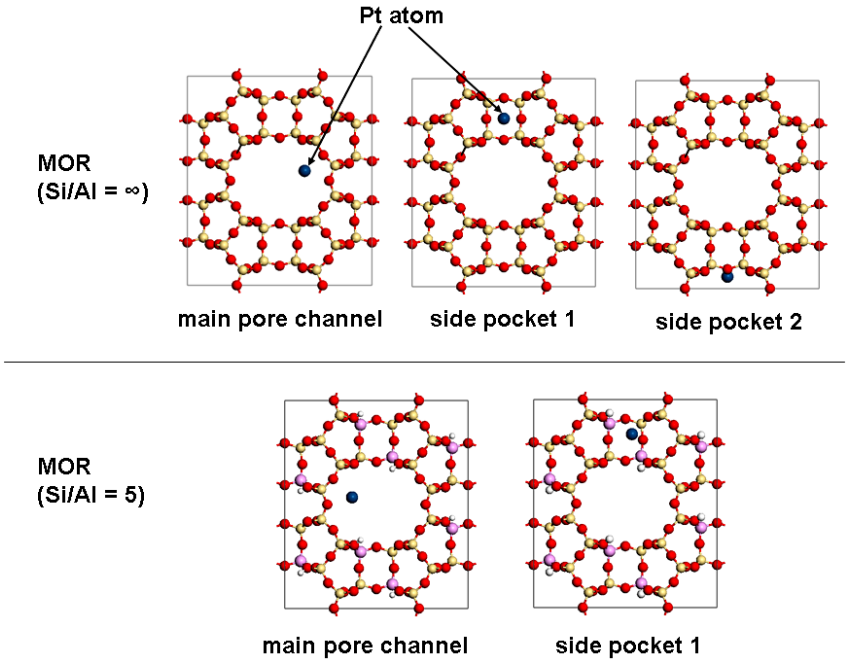

Figure 5.3 - Positioning of Pt atoms in MOR at local energy minima

Figure 5.4 shows the results for the canonical MMC simulations in MOR with Si/Al = ∞ at Pt loadings of 1, 2.5, and 5.0 % (mol/mol). These schematics present the

frequency plots generated by the path of the Pt atom obtained through the simulation. Similar results for MOR (Si/Al = 5) are presented in Figure 5.5. Notice that for the lower Pt loading (1% mol/mol), the behavior of the positioning of Pt is similar to those obtained at the same temperature for the one atom simulation. For Si/Al = ∞ and T = 298 K, the Pt atoms are positioned mainly at the side pockets of the framework. Meanwhile for Si/Al = 5 and T = 298 K, the Pt atoms were positioned at the main pore channel of the structure. It is observed in general that at low concentration, the Pt atoms remain dispersed through the zeolite framework.

Table 5.1 - Energy of one Pt atom in MOR framework pores (in kcal/mol)

System	**Total Energy**	**Δ Energy(*)**
MOR - Si/Al = ∞	- 43 011.2	0.0
+ Pt main channel	- 43 024.6	-13.4
+ Pt side pocket 1	- 43 027.7	-16.5
+ Pt side pocket 2	- 43 028.5	-17.3
MOR - S/Al = 5	- 52 891.8	0.0
+ Pt main channel	-52 903.7	-11.9
+ Pt side pocket 1	-52 902.4	-10.6
+ Pt side pocket 2	--------	----

(*) ΔEnergy = Energy of system considered minus of Energy of MOR at corresponding the Si/Al

For higher Pt loadings at both temperatures, it is observed that the Pt atoms in MOR (Si/Al = ∞) are present in both the side pockets and the main pore channels. Similar results are observed for MOR with Si/Al = 5 and T = 298 K where some Pt atoms are found in the side pockets. However, for MOR with Si/Al = 5 and T = 623 K at all

loadings, the trace of the guest atoms located them consistently in the main pore channels of the framework. It is evident from these results that Pt concentration, as well as Si/Al and temperature have an important and combined effect in the position of Pt atoms through the simulations.

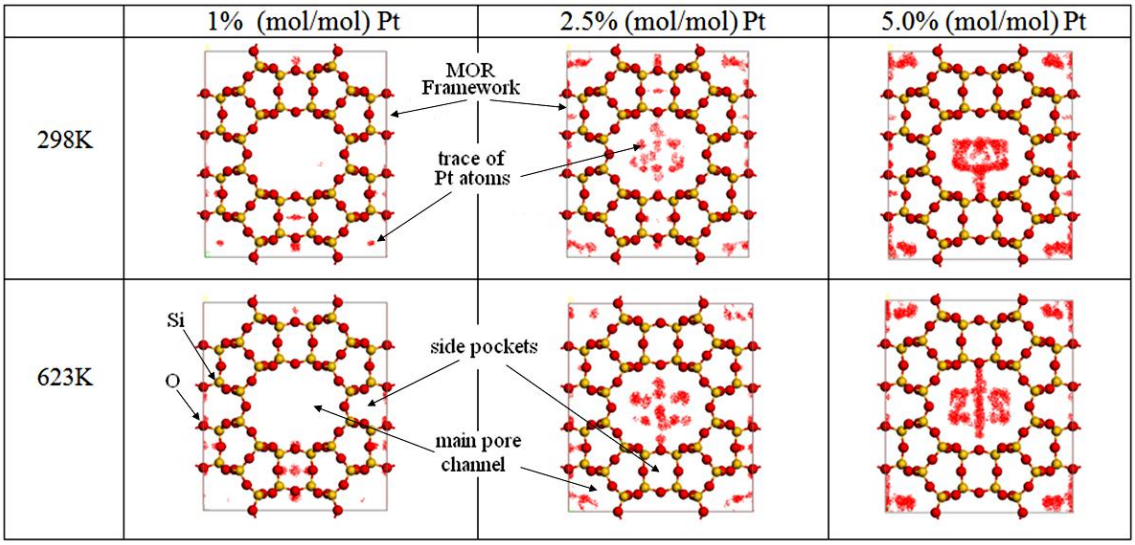

Figure 5.4 - Distribution plots for simulations of Pt in MOR (Si/Al = ∞) at different Pt loadings and temperatures (view downs the *c* axis)

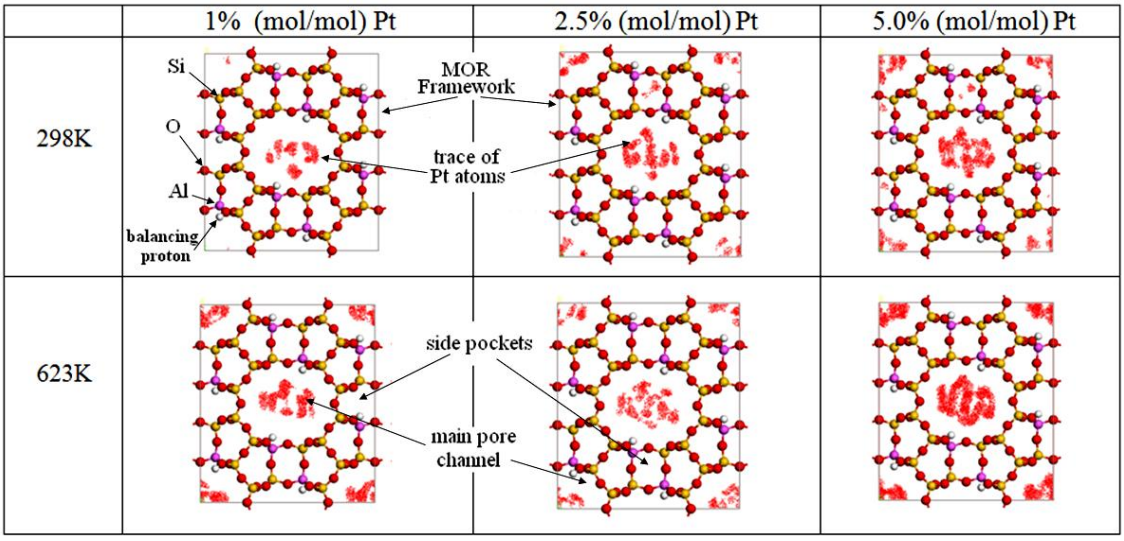

Figure 5.5 - Distribution plots for simulations of Pt in MOR (Si/Al = 5) at different Pt loadings and temperatures (view downs the *c* axis)

The increase in distribution of Pt atoms of the main pore channels at higher Pt loadings in MOR (Si/Al = ∞) can be attributed to the formation of clusters, which are energetically favored (at these loadings) in a similar fashion as the Oswald ripening effect. The size of the clusters formed then, does not allow their inclusion in the side pockets of MOR. However, Pt atoms that are distant from clusters will not be affected by its presence and will remain mainly in the side pockets of the framework.

For the specific case of MOR (Si/Al = 5) and T = 298 K, higher loadings of Pt atoms promote the displacement of guest metal atoms to the main pore channels of the framework for the same reasons explained above. In addition, at Si/Al = 5 it is expected that Pt atoms will be energetically favored to be positioned at the main pore channels and not at the side pockets of the framework. However, the displacement of Pt atoms from the side pockets to the main pore channels is affected by the size of the interconnecting ring. When the temperature is increased from 298 K to 623 K, the mobility of clusters and Pt atoms is greatly increased. This ultimately drives Pt atoms trapped in the side pockets to gain access to the main pore channels where they will remain because of the greater energetic stability at these conditions.

Figures 5.6 and 5.7 present the results obtained from the molecular dynamics simulations, by means of snapshots of the process at the beginning and ending of the simulations. As observed in Figure 5.6, the trend of the Pt atoms in MOR (Si/Al = ∞ and T = 298 K) is to move through the axial and radial directions. A few Pt atoms passed through the interconnecting rings and moved directly to the side pockets of the structure while others remained near the entrance of the interconnecting rings with some

oscillating movement near the places where geometric optimizations reported the local energy minimum for MOR at Si/Al = ∞. By observing consecutive snapshots of these simulations, it is noted that the mobility of Pt atoms through the interconnecting rings of MOR is somewhat restricted; not all Pt atoms had enough kinetic energy to pass through these rings. Notice that some metal atoms remain dispersed and a cluster is formed through the simulation period. The low mobility in the axial direction can be attributed to the attraction forces exhibited by the walls of MOR over the Pt atoms, as that the local energy minima for these Si/Al conditions are reported at the side pockets and near the walls of the main pore channel.

For the conditions of Si/Al = ∞ and a temperature of 623 K, a different displacement pattern to the one observed at 298 K was observed. While the displacement of the Pt atoms is in both the radial and the axial directions, the predominant trend is to move from the center of the main pore channel to the side pockets. The formation of a small cluster (3 atoms) is observed in one of the side pockets, but the majority of Pt atoms remain dispersed.

In the case of Si/Al = 5 and a temperature of 298 K, the displacement of the Pt atoms is observed through the axial and radial directions of the main pore channel of MOR (see Figure 5.7). However, the mobility of the Pt atoms in the axial direction is greater than mobility in the radial direction. This greater mobility in the axial direction allows Pt atoms to interact more frequently and the formation of metal clusters is observed. Some Pt atoms remain dispersed in the MOR structure through the simulation period.

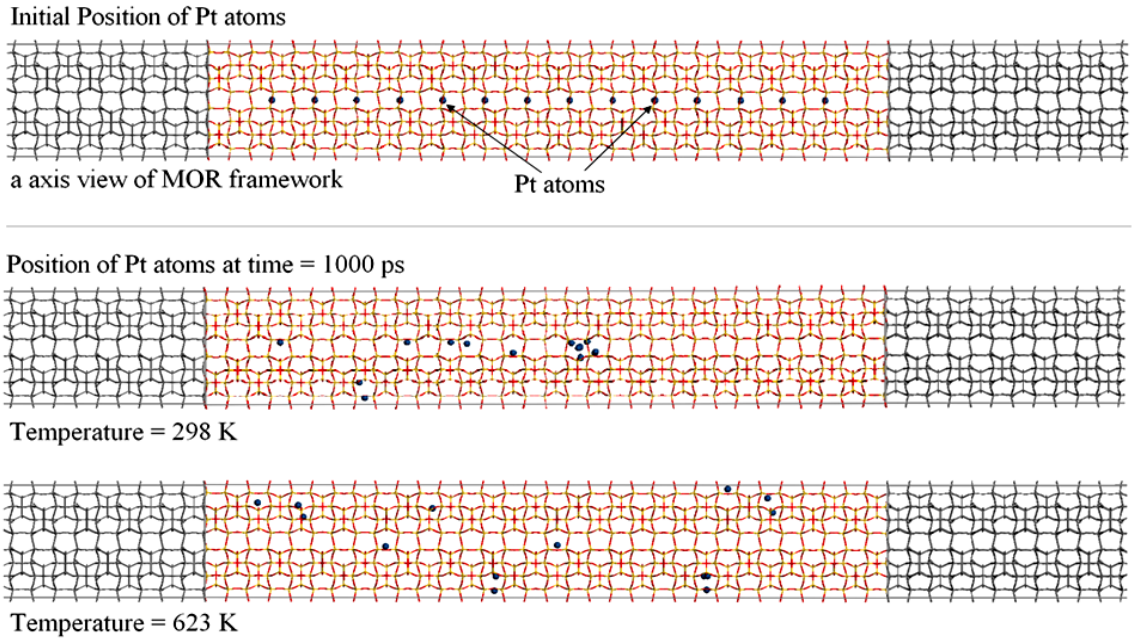

Figure 5.6 - Initial and final positions of Pt atoms in MD simulations at two simulation temperatures for MOR (Si/Al = ∞)

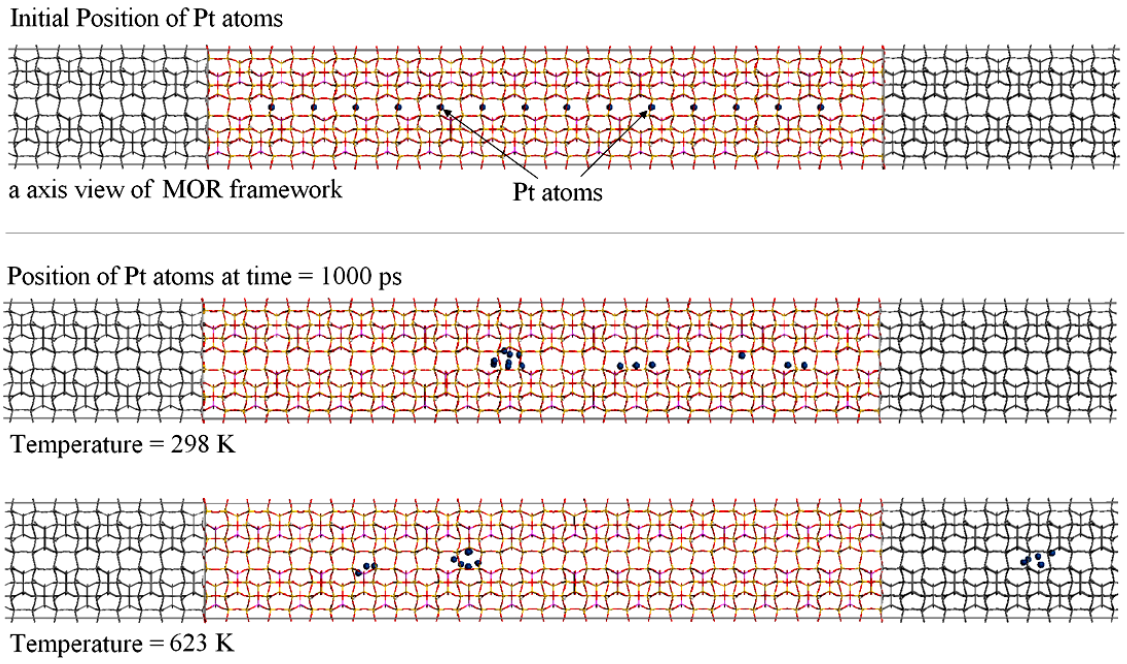

Figure 5.7 - Initial and final positions of Pt atoms in MD simulations at two simulation temperatures for MOR (Si/Al = 5)

As expected, in the case of Si/Al = 5 and a temperature of 623 K, the mobility of Pt atoms is greater than the one observed for 298 K and the same Si/Al. The tendency of the Pt atoms is to move mainly in the axial direction and more clusters are formed through the simulation period. It is interesting to observe that through these simulations, the mobility of single Pt atoms during the simulation time is relatively low, even at higher temperatures, due to the attraction forces between these atoms and the walls of the MOR structure. However, as soon as Pt clusters are formed, the attraction forces between these metal atoms maintain them apart of the walls of the main pore channels, reducing the effect of the walls in the mobility of the guest metal atoms.

The general trends observed in the MD simulations are in agreement with the results obtained for the MMC simulations at both low and high concentrations. For Si/Al = ∞, the trend of single Pt atoms is to move toward the side pockets of the MOR framework while for Si/Al = 5, the Pt atoms remain in the main pore channel of the structure. Mobility of the guest metal atoms is increased with temperature. In areas where local Pt concentration is high (i.e. where clusters are formed), the Pt atoms remain closer to the center of the main pore channel. In addition to these agreements, MD simulations also illustrate that the mobility of Pt atoms is increased when clusters are formed, thus is reasonable to expect that as high concentrations of guest metal atoms promote the formation of clusters, these same high concentrations will promote the mobility of these atoms through the MOR framework.

5.3.2 Comparison of simulations results with previous studies

Some interesting convergences are observed when comparing MMC simulation results for Pt in MOR with a recent experimental work. In experiments by Quiñones et al. [66], the formation of Pt nanowires near the surface of MOR (Si/Al = 6.5) was observed at high concentrations of $NaBH_4$, which was used as a reducing agent in the solid state. These experiments were conducted at room temperature (approximately 298 K). For these conditions, a molar ratio of $NaBH_4$/Pt = 9.8 was needed for the formation of nanowires. At an intermediate ratio of $NaBH_4$/Pt = 3.5 Pt clusters were formed inside the mordenite structure while, for $NaBH_4$/Pt = 1 no detectable Pt particles were formed. Because $NaBH_4$ was applied as a solid, the reduction of the precursor molecules $[Pt(NH_3)_4(NO_3)_2]$ probably occurred in the surface of the zeolite crystals. While all samples were impregnated with the same amount of the Pt precursor, the release of free Pt atoms is expected to occur at a faster rate for the conditions with a higher concentration of the reducing agent. Because of that, local concentration of free Pt atoms in areas near the surface of the MOR sample at the beginning of the reduction process is proportional to the concentration of the reducing agent. Simulation results presented here show that lower local metal loadings promote the dispersion of Pt atoms through the MOR structure and its inclusion in the side pockets, even at Si/Al values of 5. When higher local metal concentrations are reached, Pt particles begin to agglomerate in the main pore channels of the structure promoting the formation of bigger particles, such as clusters. If even higher local Pt concentrations are reached, it is logical that the formation of nanowires will be promoted. The higher the local concentration the lower

dispersion exhibited through the zeolite. This would explain why nanowires are formed near the surface of the zeolite crystals and not inside the framework.

With traditional templated synthesis methods, it is difficult to reach high localized metal concentrations for the formation of Pt nanowires because the precursor compound and the reduction agent would typically be uniformly distributed inside the template. Because of the size of the precursor molecules and the diameter of typical zeolite channels, local Pt concentrations inside the pores are probably too low to form nanowires. But with the solid state reduction method [66], higher local concentrations of free Pt atoms are reached because the migration of the reduction agent to the interior of the zeolite is restricted, and the reduction process occurs in specific areas near the surface.

5.4 Conclusions

The results presented here show the importance of temperature, Si/Al, and metal loading on the template synthesis of Pt nanostructures in MOR frameworks. Frequency plots of our MMC simulations indicate that high Si/Al ratios (Si/Al = ∞) favor the displacement of Pt atoms to the side pockets of the MOR framework, while at low Si/Al ratios (Si/Al = 5) the displacement of these guest metal atoms is to the main pore channels.

Also, as was expected, higher temperatures increased the mobility of Pt atoms through the framework both through the main pore channels and through the interconnecting rings. In addition, higher local Pt loadings (5% mol/mol) promote the positioning of Pt atoms in the main pore channels of MOR. These tendencies imply that

the formation of Pt nanowires will be enhanced by the use of MOR zeolite with a low Si/Al, a high metal concentration and high temperatures.

The MD simulations showed that the mobility of Pt clusters is greater than the mobility of single Pt atoms inside the main pore channels of MOR and this was explained as due to the fewer interaction of the Pt in clusters with the zeolite. These simulations also showed that a low Si/Al favors the axial diffusion of Pt atoms in the pore channels which is necessary for the formation of nanowires.

Chapter 6 - Studies of the Formation of One Dimensional Pt Structures in VET-type Zeolites

6.1 Introduction

The work presented in this chapter is focused on the formation of one dimensional Pt structures in the main pore channels of the Virginia Polytechnic Institute Eight (VET) framework. Similar to the studies presented in previous chapters, the effect of Si/Al and synthesis temperature is considered, but here it is extended to include Monte Carlo simulations under the grand canonical ensemble to obtain nanowire structures on the main pores. These structures were geometrically optimized both inside and outside the zeolite with the *pcff* forcefield, and their thermal stability was studied with molecular dynamic simulations. The most stable isolated nanowire structure was further optimized with DFT and its structure is reported.

The choice of VET is due to its small symmetrical main pore channels which are favorable for the formation of very thin symmetrical structures. It was selected over the CAN framework because preliminary simulation results for Pt were more promising and interesting. The main pore channels of VET, which have rings with 12 oxygen atoms, have a minimum distance of 5.9 Å between two opposed oxygen atoms, as shown in Figure 6.1. The windows to the side pockets of the VET structure have 6 oxygen atoms with a minimum distance between two opposed oxygen atoms in these rings of ~ 2.1 Å. The chemical formula of the zeolites with the VET framework is $Al_nSi_{17-n}O_{34}$. In the case of the Virginia Polytechnic Institute # 8 zeolite (VPI-8), the Si/Al = ∞ and the molecular

formula is reduced to $Si_{17}O_{34}$. For a VET framework with 4 Al atoms per unit cell, the Si/Al = 3.25 and the molecular formula is $Al_4Si_{13}O_{34}$. [60]

6.2 Simulation Methodology

Metropolis Monte Carlo (MMC) simulations under the canonical and grand canonical ensembles were done with the Sorption module of Materials Studio Software™, Version 4.0 (Accelrys, Inc., San Diego, California, USA). For the molecular dynamics simulations, the Forcite Plus module of Materials Studio (version 5.5) was used. All MMC simulations were performed with 2 x 10^6 equilibration steps, 1 x 10^7 processing steps and a maximum displacement set to 1.0 Å.

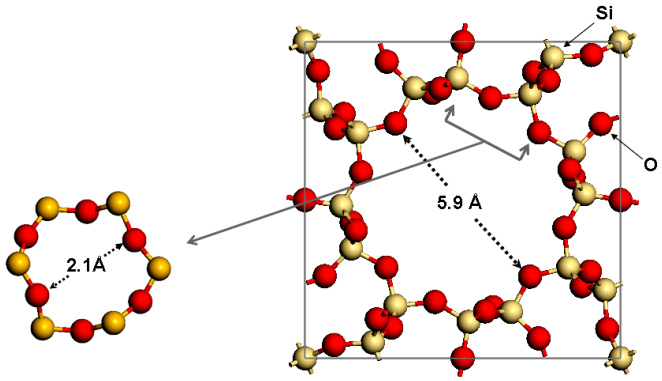

Figure 6.1 - VET Framework (Si/Al = ∞)

Unless otherwise stated, energy computations for these simulations and geometric optimizations were done using the *pcff* forcefield developed by Sun et al. [82,83] A cut off ratio of 18.5 Å was used for energy computations, with a cubic spline truncation set to 1.0 Å and a buffer set to 0.5 Å .

6.2.1 Supercell definition and the positioning of the Al atoms in VET

For the MMC simulations, the VET framework was used with Si/Al = ∞ and Si/Al = 3.25. The supercell of VET was composed of 1 x 1 x 16 unit cells (containing 816 atoms). The relative position of the atoms in the VET framework was fixed during the simulation period. For the positioning of the Al atoms in VET with Si/Al = 3.25, several configurations were evaluated. In each of them, one Al atom per primitive cell was located at one of the five unique tetrahedral sites available (see Figure 6.2). The unit cell with Al atoms at the T2 sites was selected, as it resulted in the most stable configuration. To establish the position of the charge-balancing protons a similar approach was used, as geometric optimizations were done for the several configurations selecting the ones that resulted in the lowest energy. Specific details related to this procedure are described in previous chapters.

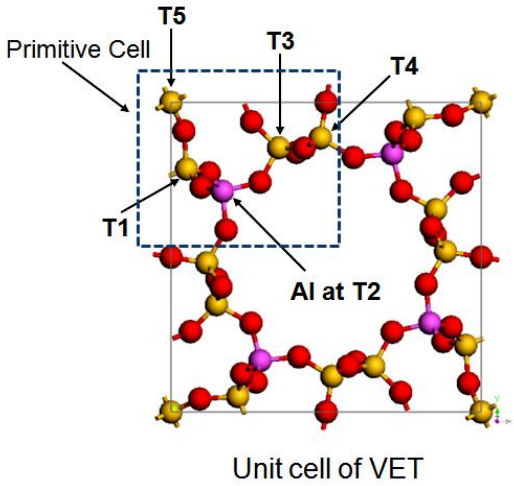

Figure 6.2 - Tetrahedral sites available in the VET for the positioning of Al atoms

6.2.2 MMC simulations and geometric minimizations of one Pt atom in VET

MMC simulations were performed with a loading of one Pt atom in order to study the interaction between Pt and the VET framework at two different Si/Al (∞ and 3.25) and two temperatures (298 and 623 K). Geometric optimizations were also done with this loading and Si/Al ratios to find the most stable locations of the Pt in the main pore channels and side pockets of VET. For these geometric optimizations, the relative position of the zeolite atoms was fixed. Specific details of these procedures are described in previous chapters.

6.2.3 MMC simulations for VET under the grand canonical ensemble

Evaluation of the distribution of Pt atoms within the VET framework at Si/Al=3.25 and ∞ and T=298 K and 623 K was done using grand canonical Monte Carlo (GC-MC) simulations. These simulations were done to encourage the formation of one dimensional Pt structures within the VET framework and to obtain the most stable configurations. After running the simulations, the configurations with the lowest energy were geometrically optimized; then, the VET framework was removed and the isolated Pt structure was again geometrically optimized.

6.2.4 Stability of one dimensional Pt structures

The thermal stability of the isolated optimized Pt structures obtained in section 5.2.3 was studied with molecular dynamics simulations at 50, 100, 125 and 150 K. The time step for each of the iterations was fixed to 1 fs and the total simulation time was set to 10^4 ps, resulting in 1 x 10^7 simulation steps. The temperature was fixed using the

NOSE thermostat algorithm and the initial velocities of Pt atoms were assigned randomly.

6.2.5 Geometric optimizations of Pt structure with DFT

The formation of a larger Pt nanostructure was promoted inside a VET supercell of 36 unit cells at Si/Al = 3.25 and T = 623 K using the methodology described in section 6.2.3. The structure was then optimized both inside and outside the VET framework using the methodology described in the same section. The resulting isolated structure was further optimized using DFT in order to compare deviations of size, shape and distance between atoms. The DFT geometric optimizations were done with Dmol[3] software of Accelrys, Inc., San Diego, California, USA. For the DFT energy calculations, the Perdew–Burke–Ernzerhof (PBE) exchange and correlation functionals were used and the Kohn-Sham orbitals were expanded in double numerical plus polarization (DNP) basis set.

6.3 Results and Discussion

Figure 6.3 presents the distribution plots of the MMC simulations for one Pt atom in VET at the different Si/Al and temperatures studied. In all the figures, the path of the Pt atom remained inside the main pore channel of the framework. The path of the Pt atom for Si/Al = ∞ and T = 298 K suggests that there are very specific places near the surface of the pore walls that are energetically favored for its positioning. For the case when Si/Al = 3.25 and T = 298 K, the preferred position of the Pt atom is displaced to the

center of the main pore channels. The differences exhibited at these two conditions suggests that zeolite walls have a much lower restrictive effect on the mobility of the Pt atom in the axial direction at Si/Al = 3.25. The tendency of Pt of moving away from the walls of the zeolite pore at low Si/Al ratios is similar to the behavior discussed in previous chapters on the CAN and MOR frameworks.

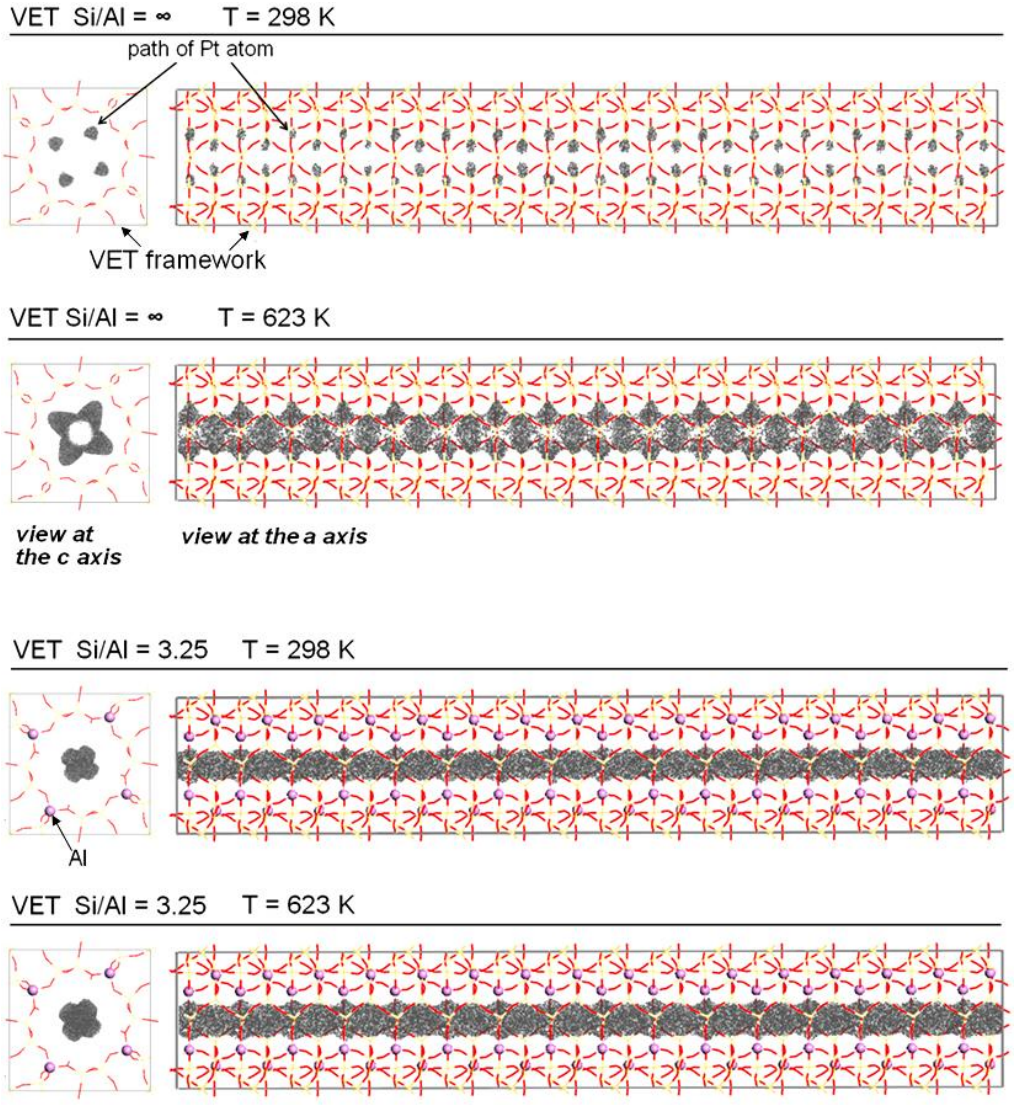

Figure 6.3 - Distribution plots of one Pt atom in VET framework (MMC simulations)

For the case of VET with Si/Al = ∞ and T = 623 K, the path of the Pt atom illustrates the acceptance of the random walk through places that were not favored at T = 298 K. This new path suggests a continuous rather than an interrupted travel of the Pt atom. For Si/Al = 3.25 at T = 623 K, the path of the Pt atom through the random walk is similar to the one observed at T = 298 K; however, there is a slight increase in the radial displacement of the Pt atom through the main pore channel.

Figure 6.4 and Table 6.1 present the geometric minimization results for one Pt atom inside the VET framework. As explained in other chapters, the values of ΔE correspond to the difference between the energy of the VET framework and the Pt atom at its optimized geometry and the energy of the VET framework alone. The values of ΔE and the position of the Pt atom at its local minima are in accordance with the results obtained for the MMC with one Pt atom. For VET with Si/Al = ∞, ΔE is lower at the local minima found in the main pore channel than ΔE at the local minimum found in the side pockets. Also, the value of ΔE for Pt at the side pockets is positive, which implies that it is unlikely to find Pt atoms at this position. When Si/Al = 3.25, the position of Pt at the local energy minima is shifted from near the wall to the center of the main pore channel. There are in fact two local minima found under these conditions, one in the center of the main pore channel and the other near the center but slightly shifted to the wall. There is also a local energy minimum in the side pocket of the Si/Al = 3.25 VET framework, but it has a positive ΔE value. The position of Pt at this local energy minimum is almost the same to the one on the Si/Al = ∞ although with a higher value of ΔE which makes it more unlikely to find Pt atoms there.

Results for the GC-MC simulations with geometry optimizations are presented in Figure 6.5. In all the simulations, the main pore channel of the zeolite frameworks was filled with Pt atoms which formed nanowire like structures.

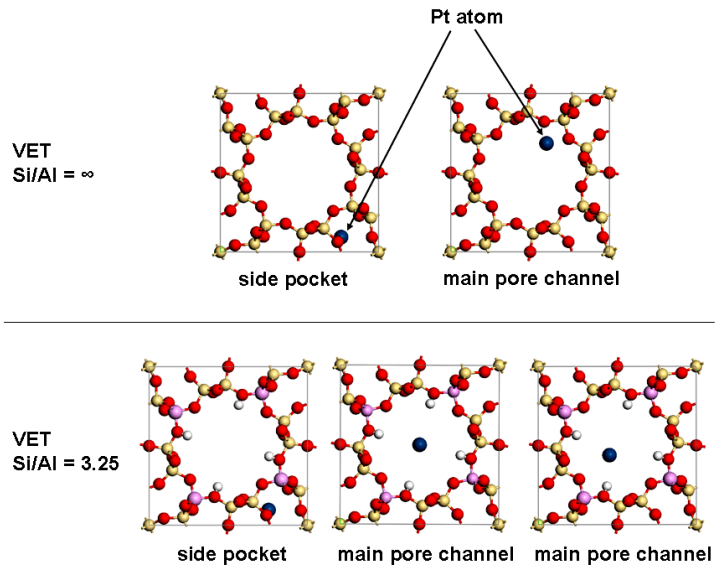

Figure 6.4 - Positioning of Pt atoms in VET at local energy minima

Table 6.1 - Energy of one atom of Pt in VET framework pores (in kcal/mol)

System	Total Energy	Δ Energy(*)
VET- Si/Al = ∞	-10 843.0357	0.0000
+ Pt main channel (center)	----------	----------
+ Pt main channel (near wall)	-10 858.5918	-15.5561
+ Pt side pocket	-10 833.8875	9.1482
VET- Si/Al = 3.25	-20 510.1064	0.0000
+ Pt main channel (center)	-20 518.0712	-7.9648
+ Pt main channel (near wall)	-20 518.2563	-8.1499
+ Pt side pocket	-20 439.1242	70.9822

(*) ΔEnergy = Energy of system considered minus Energy of VET at the corresponding Si/Al

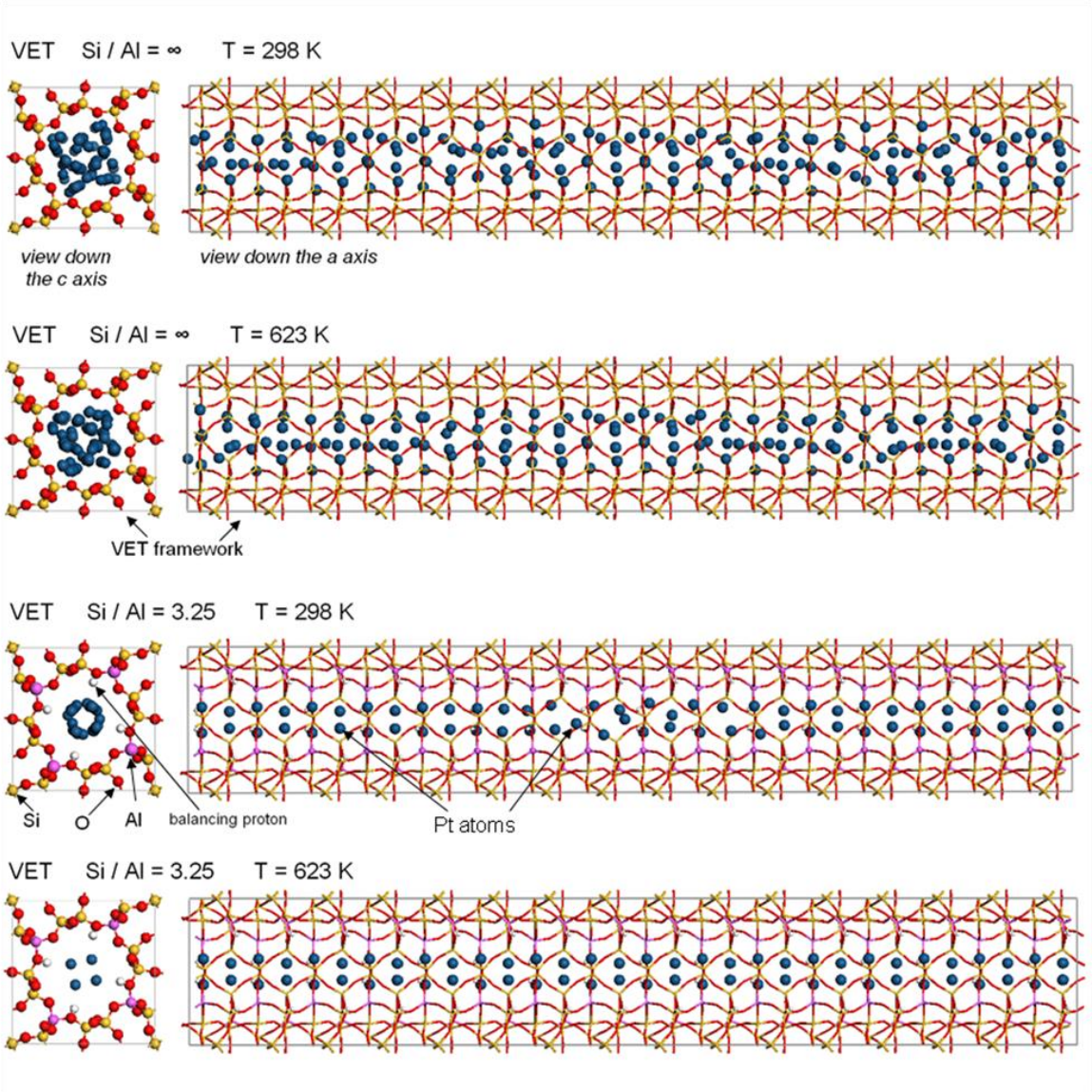

Figure 6.5 - Location of Pt atoms at their minimum energy configurations in VET after GC-MC simulations and GO

The schematics in the left column of Figure 6.6 show the one dimensional Pt structures formed inside VET after geometric optimization. Notice that for the specific case of Si/Al = 3.25 and T = 623 K, the Pt atoms present a more ordered pattern than those observed at the other simulated conditions. It seems that at this temperature and

Si/Al ratio the increased mobility of Pt atoms and the repulsion of the zeolite main pore channel allow the Pt atoms to reach the local minimum positions found during the geometry optimization of one Pt atom in this same zeolite, resulting in a more ordered atomic configuration. At T = 298 K and a VET framework with the same Si/Al ratio, the one dimensional Pt structure obtained have some segments with a similar atomic arrangement to the one formed at T = 623 K, but in general it was disordered.

The Pt structures obtained at Si/Al = ∞ exhibited, in general, a disordered pattern. This behavior can be explained by the lower repulsion exhibited between the walls of the zeolite, which permitted the introduction of more Pt atoms thorough the GC-MC simulation. The combination of the presence of more Pt atoms and the lower interaction with the walls of the zeolite diminished the capacity of the zeolite to template an ordered structure.

The right column of Figure 6.6 presents schematics of the results obtained from geometric optimizations of the one dimensional Pt structures after removing the VET framework. For the specific case of VET with Si/Al = 3.25 and T = 623 K, the obtained one dimensional Pt structure after geometry optimization outside the VET framework present an ordered (but not crystalline) pattern, that can be classified as quasicrystal. The results obtained for the other three conditions did not present any ordered pattern.

Molecular dynamics simulations performed for the four one dimensional Pt structures at 50, 100, 125 and 150 K indicated that all structures, with the exception of the one formed at Si/Al = 3.25 and T = 623 K, collapsed at all temperatures studied forming a much compact cluster-like structure. For the one dimensional Pt structure

formed at Si/Al = 3.25 and T = 623 K, the ordered structure maintained its integrity up to T = 125 K.

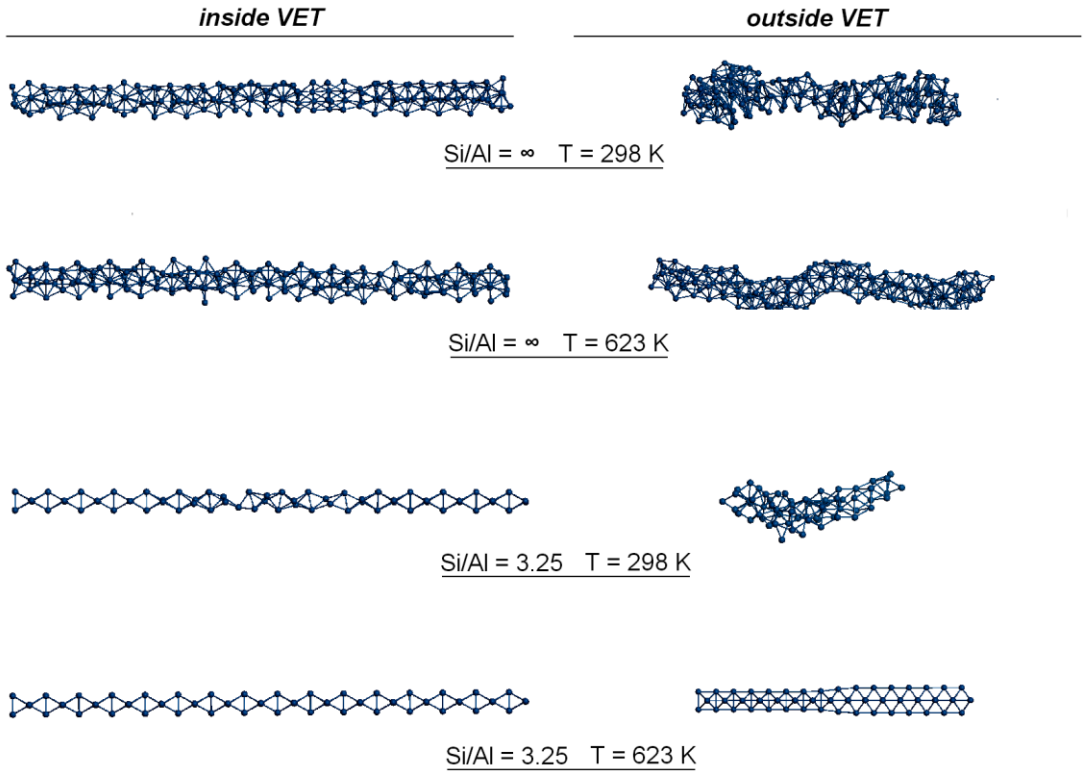

Figure 6.6 - Geometric optimizations of Pt structures inside and outside VET

Figure 6.7a shows a three dimensional view of the longer Pt nanowire-like structure formed at Si/Al=3.25 and T=623K using a supercell of 36 VET unit cells (as described in section 6.2.5) after geometric minimization with *pcff*. This structure resembles the one reported by Peng et al. [112] for the case of Ni after relaxation of the structure labeled (4,2) using molecular dynamics at 0 K with the EAM potential. [117] In that study, the unrelaxed and relaxed structures of Ni are similar to the Pt structures obtained inside and outside VET, respectively (for Si/Al = 3.25 and T = 623 K). While these similarities are not surprising, as Ni and Pt are transition metals of the group VIIB

(in the periodic table), it is important to emphasize that the structure reported by Peng et al. was obtained from the relaxation of a theoretical structure proposed by symmetry and not from a simulation based on an existing template. Our results then suggest that it is possible to experimentally obtain theoretically proposed structures by using zeolites as templates. As mentioned in the introduction, deviation of crystalline patterns to regular but unusual patterns in metal nanowires was predicted Gülseren et al.. [109] These wires presented large irregularities that depended on the nanowire thickness. Some of the formed wires have helical structures. The authors attributed the observed deviations to the competition of two predominant energy effects, the optimal internal packing and the minimal surface energy. If the radius of the nanowire is smaller than a critical value, the minimal surface energy effect predominates over optimal internal packing effect and deviations to crystalline patterns start to appear. In that study the authors used only interatomic potentials for their energy calculations; however they pointed out the importance of effect of electronic shells effects in the final positioning of metal atoms, especially for nanowire structures of very small radii.

Figure 6.7b presents the Pt nanowire after geometric minimization using DFT. Notice that there is a slight shift in the alignment of the Pt atoms, giving a curved or wavy path of the whole nanowire structure. This wavy path is similar to the one reported by Oshmima et al. for the synthesis of thin gold nanowires. [128]

Figure 6.8 shows the details of the structures formed after both, *pcff* and DFT geometric optimizations. When comparing the interatomic distances between the two structures it is evident that those obtained by DFT optimization are smaller. The distances obtained by DFT are in accordance to those reported for small nanostructures,

a) GO of Pt nanowire with *pcff* outside VET

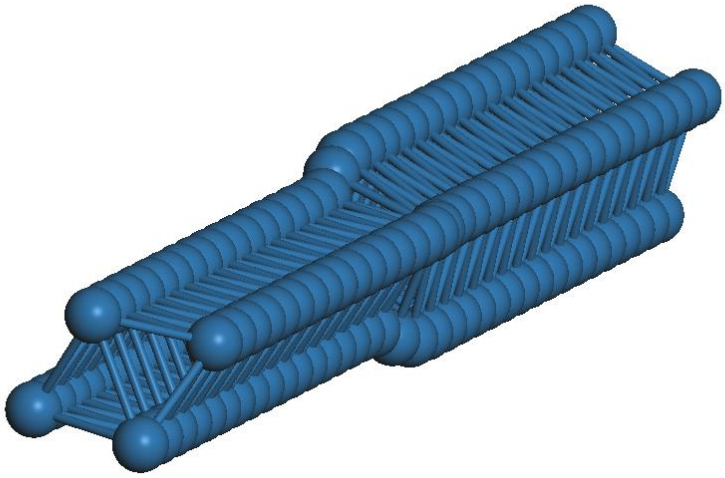

b) GO of Pt nanowire with *DFT* outside VET

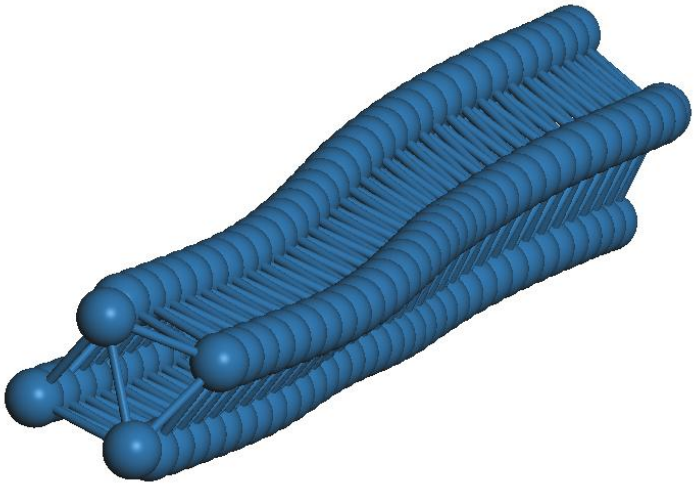

Figure 6.7 - Geometric optimizations of one dimensional Pt structures with *pcff* and *DFT*

while the distances reported by *pcff* are more similar to the values reported in the bulk. While the forcefield is not capable to estimate precise distances between these metal atoms in nanostructures, it seems to be adequate to give a qualitative description of how these atoms are positioned in space, at a low computational cost.

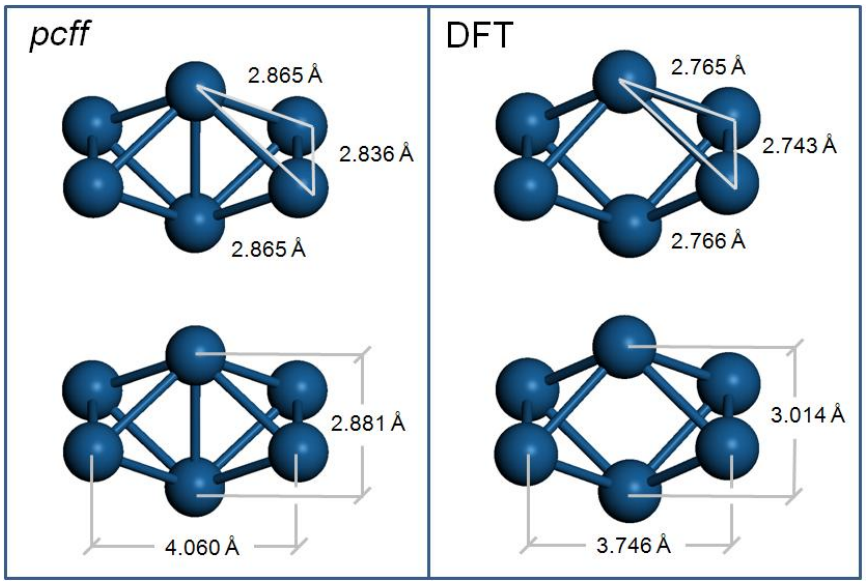

Figure 6.8 - Distances between atoms in the optimized Pt structures with *pcff* and DFT

6.4 Conclusions

The results presented suggest that, theoretically, it is possible to obtain thermally stable ordered one dimensional Pt nanostructures using a VET zeolite. It was shown that the formation of these ordered structures depends strongly on synthesis parameters such

as temperature and Si/Al, and that Si/Al = 3.25 and T = 623 K were the optimal parameters found of those studied. These ordered structures exhibit good structural and thermal stabilities, which are essential to maintain the integrity of these ultrathin nanowires.

This study also shows that it might be possible to experimentally obtain ultrathin nanowires predicted by theoretical methods using VET zeolites as templates. The results also suggest it might be possible to extend these results to similar one dimensional zeolite frameworks; i.e. with symmetrical one dimensional pore channels and side pockets with small windows, under similar synthesis conditions. Finally, this study suggests that *pcff* geometry optimization can be used to obtain reliable one dimensional Pt structures at low computational costs.

Chapter 7 - Analysis, Discussion and Recommendations

7.1 Analysis and Discussion

The results presented through this dissertation are based on simulations of neutral metal atoms and their interaction with zeolite frameworks, under conditions that simulate the final steps of templated synthesis methods in which ultrathin nanowires could be formed. Effects associated with the inclusion of other particles (such as molecules or ions) through the synthesis process are not considered, so the reader must be take into consideration that the following comments are done in the context of the limits in which the study was realized.

Comparing the results and conclusions of Chapters 4 to 6 of this dissertation, key aspects necessary for the successful synthesis of nanowires in zeolites were identified. In terms of the framework type, it is clear that the size of the interconnecting windows between the main pores and the side pockets must be taken into consideration, when selecting zeolites as templates for experimental work. When these windows are large enough, migration of metal atoms from the main pore channels to side pockets can occur. This migration could have detrimental effects on templated synthesis of metal nanowires, because it is on the main pore channels where they could be formed.

We have seen that Si/Al has an important effect on the positioning of neutral metal atoms in a zeolite. For lower values of Si/Al, the positioning of metal atoms inside the main pore channels is energetically favored over the side pockets, while the opposite is true for very high values of Si/Al. This fact helps to reduce the displacement of metal

guest atoms from the main channels to the side pockets in zeolites such as mordenite, which has interconnecting windows large enough to allow migration of metal atoms outside the main pore channels.

This effect is related to the one observed in Chapter 4, where the results obtained with the MMC simulations evidences that the presence of Al atom in the zeolite framework promotes the separation of the guest metal atoms from the wall surfaces of the zeolite structure. In terms of energetic stability, this means that the stability of guest metal atoms inside the zeolite framework is achieved farther away from the O atoms around an Al atom than the O atoms around a Si atom. The result is that, as the number of Al atoms in the zeolite framework increases (i.e. the Si/Al decreases) the distribution of the metal atoms through the zeolite framework becomes more uniform. As seen in Chapter 5, this effect has a direct influence on the diameter of the nanowires formed inside the pore channels, but more importantly in the relative position between these metal atoms, influencing the final structure and stability of the nanowires removed from the template.

Another important factor studied in Chapters 3 and 4 was the metal loading. As concluded in these chapters, higher metal loadings promote the formation of aggregates inside the pores of zeolites, while low concentrations promote dispersion of metal atoms through their framework. This effect can be physically explained by the fact that the agglomeration of metal atoms is thermodynamically favored (in a similar fashion as the Oswald ripening effect). But in order to agglomerate, these particles must interact first; the probability of interaction between guest metal atoms in the zeolite is increased with an increase in metal loading. For low metal loadings, the probability of interaction is

smaller and thus, these particles remain disperse. For the case where agglomeration occurs, bigger particles require more space and they remain in the main pore channels due to energetic considerations.

It is important to emphasize that, in terms of this research made with molecular simulations, metal loadings are local loadings. To achieve high local metal loadings in actual templated synthesis, it is important to select proper methods for incorporation of metal atoms in the zeolite framework. In the specific case of wet impregnation and synthesis by reduction, metal organic salts are typically used as precursors. Metal ligands occupy space reducing the interaction between metal atoms. Also, it is expected that the size and shape of the metal ligands have an important effect, as diffusion of these particles inside the pores can be restricted by these factors.

Temperature has a very important effect in the formation of nanostructures because higher temperatures increase mobility of guest atoms. The increase in mobility of atoms can have a positive or negative effect on the formation of nanowires, depending on its magnitude and the effect of other variables such as framework type, Si/Al and metal loading. In general, if other variables are managed to provide a stability of metal atoms inside the main pore channels of the zeolite, an increase in temperature has a positive effect in the formation of metal nanowires because guest atoms can interact more frequently, increasing the possibility of forming elongated structures. Also the higher mobility at higher temperatures seems to help metal atoms reach stable positions inside the pores, forming more ordered and stable one dimensional structures.

The results presented throughout this dissertation suggest that it is possible to obtain thermally stable ordered one dimensional metal nanostructures using proper

zeolite frameworks and correctly managing parameters such as Si/Al, metal loading, and temperature. They also show that it might be possible to use zeolites to experimentally obtain ultrathin nanowires with ordered structures previously predicted by theoretical methods.

Finally, this study showed that geometric optimizations using the *pcff* forcefield can be used to obtain qualitatively correct one dimensional Pt nanostructures at low computational costs compared to *ab initio* methods. This suggests that this forcefield can be used as a reliable method to obtain configurations of nanostructures in zeolites.

Overall molecular simulations were able to give us guidelines that can be used to the successful synthesis of nanowires using zeolites as templates.

7.2 Recommendations for Future Studies

Simulation studies are important scientific tools that help explain natural phenomena and provide theoretical basis to be used in predictions and overall design of practical applications. However, it is always good practice to complement theoretical studies with experimental observations and vice versa, in a dynamic that always brings new answers, but more important, new questions. For that reason, the first suggestion is to perform experimental research to confirm the observed effects of the variables studied in this dissertation over the templated synthesis of metal nanowires using zeolites.

The research methodologies used in the present study have proved to be useful to predict, in theoretical bases, the capacity of a zeolite framework to *cast* metal nanowires with specific patterns of arrangement of atoms. Because of the importance of this

information for the design of experimental work, our second recommendation is to perform research using these methodologies to generate a database of possible metal ultrathin nanowires (and other nanostructures) that can be synthesized with the frameworks reported by the International Zeolite Association (IZA). This database will help researchers to select zeolite frameworks and metals for impregnation to perform experimental research, according to their specific needs.

One of the typical problems after the synthesis of any nanostructure is the agglomeration (and possible deformation) of the particles after removal from the template. One way to prevent this effect is by embedding some type of coating material that prevents contact between the synthesized nanoparticles. In the case of ultrathin metal nanowires, this could represent a major difficulty when performing the actual synthesis and posterior removal of the template. However, an interesting possibility to overcome this problem could be to use side pockets of zeolites like mordenite as storage (prior to synthesis) of the coating material. The implementation of such technique would require knowledge of the adsorption behavior of the selected coating materials in the selected zeolite. Based on that, our last recommendation is to do research using molecular simulations to study the adsorption of materials that could be used for coating purposes.

References

1. M. C. Roco, *Nanoscale Science and Engineering: Unifying and Transforming Tools*, AICHE Journal, 50:5, 2004, p.p. 890-897

2. I.D. Marinescu, J. Ramírez-Salaz, A. A, Noreyan, *New Millennium frontiers on precision engineering*, Int. J. Prod. Res., 40:15, 2002, p.p. 3807-3819

3. J. Panyam, V. Labhasetwar, *Sustained Cytoplasmic Delivery of Drugs with Intracellular Receptors Using Biodegradable Nanoparticles*, Mol. Pharmaceutics, 1:1, 2004, p.p.77-84

4. L. Collins, M., Kaszuba, J. W. Fabre, *Imaging in solution of $(Lys)_{16}$- containing bifunctional synthetic peptide/DNA particles for gene delivery*. Biochimica et Biophysica Acta, 1672:1, 2004, p.p. 12-20

5. V.P. Zarov, R. R. Letullin, E. N. Galitovskaya, *Microbubbles-overlapping mode for laser killing of cancer cells with absorbing nanoparticle clusters*, J. Phys. D: Appl. Phys. 38, 2005, p.p. 2571-2581

6. Y. Zhang, N. Kohler, M. Zhang, *Surface modification of superparamagnetic magnetite nanoparticles and their intracellular uptake*, Biomaterials 23:7, 2002, p.p. 1553-1561

7. S. Hrapovic, Y. Liu, K. B. Male, J. H. Luong, *Electrochemical Biosensing Platforms Using Platinum Nanoparticles and Carbon Natotubes*, Anal. Chem., 76:4, 2004, p.p. 1083-1088

8. R. W. J. Scott, O. M. Wilson, R. M. Crooks, *Synthesis, Characterization, and Applications of Dendrimer-Encapsulated Nanoparticles*, J. Phys. Chem. B, 109:2, 2005, p.p. 692-704

9. A. Moser, K. Takano, D.T. Margulies, M. Albrecht, Y. Snobe, Y. Ikeda, S. Sun, E. Fullerton, *Magnetic recording: advancing into the future*, J. Phys. D: Appl. Phys., 35, 2002, p.p. R157-R167

10. R. Elghanian, J. J. Storhoff, R. C. Mucic, R. L. Letsinger, C.A. Morking, C. A., *Selective colorimetric detection of polynucleotides based on the distance-dependent optical properties of gold nanoparticles*, Science, 277:5329, 1997, p.p. 1078-1082

11. L. Hu, X. Cao, J. Yang, M. Li, H. Hong, Q. Xu, J. Ge, L. Wang, J. Lu, L. Chen, G. Hongwei, *Oxidation of benzylic compounds by gold nanowires at 1 atm O_2*, Chem. Commun., 47 (2011), p.p. 1303-1305

12. E. Roduner, *Size matters: why nanomaterials are different*, Chem. Soc. Rev, 35, 2006, p.p. 583-592

13. A. A. Ansari , M. N. Khan, M. Alhoshan, A.S. Aldwayyan, M.S. Alsalhi, *Chapter 1- Nanostructured Materials: Classification, Properties, Fabrication, Characterization and their Applications in Biomedical Sciences*, in *Nanoparticles: Properties, Classification, Characterization, and Fabrication (Nanotechnolgy Science and Technology)*, A. E. Kestell, G. T. Dolerey, eds., Nova Science Pub Inc , 2010, p.p. 1-78

14. L. Cademartiri and G. A. Ozin, *Ultrathin Nanowires—A Materials Chemistry Perspective*, Adv. Mater., 21 (2009), p.p. 1013–1020

15. Koenigsmann, C., Santulli, A. C., Gong, K, Vukmirovic, M. B., Zhou, W., Sutter, E., Wong, S. S., Adzic, R. R., *Enhanced Electrocatalytic Performance of Processed, Ultrathin, Supported Pd Pt Core_Shell Nanowire Catalysts for the Oxygen Reduction Reaction*, J. Am. Chem. Soc., 133 (2011), p.p. 9783–9795

16. Y. Cui, Q. Wei, H. Park, C. M. Lieber, *Nanowire Nanosensors for Highly Sensitive and Selective Detection of Biological and Chemical Species*, Science, 293 (2001), p.p. 1289-1292

17. C. M. Lieber, *Nanoscale Science and Technology: Building a Big Future from Small Things*, MRS Bulletin, July 2003

18. J. I., Pascual, J. Méndez, J. Gómez-Herrero, A. M. Baró, N. García, U. Landman, W. D. Luedtke, E. N. Bogachek, H. P. Cheng, *Properties of Metallic Nanowires: From Conductance Quantization to Localization*, Science, 67: 24 (1995), p.p. 1793-1795

19. M. S., Dresselhaus, G. Chen, M. Y. Tang, R. G. Yang, H. Lee, D. Z. Wang, Z. F. Ren, J. P. Fleurial, P. Gogna, *New Directions for Low-Dimensinal Thermoelectric Materials*, Adv. Mater., 19 (2007), p.p. 1043-1053

20. X. Teng, W. Q. Han, W. Ku, M. Hucker, *Synthesis of Ultrathin Palladium and Platinum Nanowires and a Study of Their Magnetic Properties*, Angew. Chem. Int. Ed., 47 (2008), p.p. 2055-2058

21. K. Y. Arutyunov, *Negative magnetoresistance of ultra-narrow superconducting nanowires in the resistive state*, Phys. C, 468 (2008), p.p. 272-275

22. A. A. Nikolaeva, L. A. Konopko, T. E. Huber, E. P. Sineavsky, R. A. Khamidullin, R., A. C. Tsurkan, *Negative magnetoresistance in transverse and longitudinal magnetic fields in Bi nanowires*, Journal of Physics: Conference Series, 150 (2009), p.p. 022065-022069

23. Y. N. Xia, P. D. Yang, Y. G. Sun, Y. Y. Wu, B. Mayers, B. Gates, Y. D. Yin, F., Kim, Y. Q. Yan, *One-Dimensional Nanostructures: Synthesis, Characterization, and Applications*, Adv. Mater., 15:5 (2003), p.p. 353-389

24. S. Romanov, *Electronic structure of the minimum-diameter Tl, Pb and Bi quantum wire superlattices*, J. Phys.: Condens. Matter, 5:8 (1993), p.p. 1081-1090

25. N. R. B. Coleman, M. A. Morris, T. R. Spalding, J. D. Holmes, *The Formation of Dimensionally Ordered Silicon Nanowires within Mesoporous Silica***,** J. Am. Chem. Soc., 123 (2001), p.p . 187-188

26. N. R. B. Coleman, N. O'Sullivan, K. M. Ryan, T. A. Crowley, M. A. Morris, T. R. Spalding, D. C. Steytler, J. D. Holmes, *Synthesis and Characterization of Dimensionally Ordered Semiconductor Nanowires within Mesoporous Silica*, J. Am. Chem. Soc., 123 (2001), p.p. 7010-7016

27. T. A. Crowley, K. J. Ziegler, D. M. Lyons, D. Erts, H. Olin, M. A. Morris, J. D. Holmes, *Synthesis of Metal and Metal Oxide Nanowire and Nanotube Arrays within a Mesoporous Silica Template*, Chem. Mater., 15 (2003), p.p. 3518-3522

28. K. J. Ziegler, B. Polyakov, J. S. Kulkarni, T. A. Crowley, K. M. Ryan, M. A. Morris, D. Erts, J. D. Holmes, *Conductive films of ordered nanowire arrays*, J. Mater. Chem., 14 (2004), p.p. 585-589

29. Z. Liu, Y. Sakamoto, T. Ohsuna, K. Hiraga, O. Terasaki, C. H. Ko, H. J. Shin, R. Ryoo, *TEM Studies of Platinum Nanowires Fabricated in Mesoporous Silica MCM-41*, Angew. Chem. Int. Ed., 39 (2000), p.p. 3107-3110

30. A. Fukuoka, Y. Sakamoto, S. Guan, S. Inagaki, N. Sugimoto, Y. Fukushima, K. Hirahara, S. Iijima, M. Ichikawa, *Novel Templating Synthesis of Necklace-Shaped Mono- and Bimetallic Nanowires in Hybrid Organic−Inorganic Mesoporous Material,* J. Am. Chem. Soc., 123 (2001), p.p. 3373-3374

31. M. Law, J. Goldberger, P. D. Yang, *Semiconductor Nanowires and Nanotubes*,Annu. Rev. Mater. Res., 34 (2004), p.p. 83-122

32. Z. Huo, C.-K. Tsung, W. Huang, X. Zhang, P. Yang, *Sub-Two Nanometer Single Crystal Au Nanowires*, Nano Lett., 8 (2008), p.p. 2041-2044

33. J. D. Holmes, K. P. Johnston, R. C. Doty, B. A. Korgel, *Control of Thickness and Orientation of Solution-Grown Silicon Nanowires*, Science, 287 (2000), p.p. 1471-1473

34. Y. Wu, Y. Cui, L. Huynh, C. J. Barrelet, D. C. Bell, C. M. Lieber, *Controlled Growth* and *Structures of Molecular-Scale Silicon Nanowires*, Nano Lett., 4 (2004), p.p. 433-436

35. J. W. Grebinski, K. L. Hull, J. Zhang, T. H. Kosel, M. Kuno, *Solution-Based Straight and Branched CdSe Nanowires*, Chem. Mater., 16 (2004), p.p. 5260-5272

36. M. Kuno, O. Ahmad, V. Protasenko, D. Bacinello, T. H. Kosel, *Solution-Based Straight and Branched CdTe Nanowires*, Chem.Mater., 18 (2006), p.p. 5722-5732

37. S. A. Johnson, D. Khushalani, N. Coombs, T. E. Mallouk, G. A. Ozin, J., *Polymer mesofibres,* Mater. Chem., 8 (1998), p.p 13-14

38. X. Lu, M. S. Yavuz, H.-Y. Tuan, B. A. Korgel, Y. Xia, *Ultrathin Gold Nanowires Can Be Obtained by Reducing Polymeric Strands of Oleylamine−AuCl Complexes Formed via Aurophilic Interaction*, J. Am. Chem., Soc., 130 (2008), p.p. 8900-8901

39. C. Wang, Y. Hu, C. M. Lieber, S. Sun, *Ultrathin Au Nanowires and Their Transport Properties*, J. Am. Chem. Soc., 130 (2008), p.p. 8902-8903

40. B. H. Hong, S. C. Bae, C. W. Lee, S. Jeong, K. S. Kim, *Ultrathin Single-Crystalline Silver Nanowire Arrays Formed in an Ambient Solution Phase*, Science, 294 (2001), p.p. 348

41. K. J. Ziegler, P. A. Harington, K. M. Ryan, T. Crowley, J. D. Holmes, M. Morris, *Supercritical fluid preparation of copper nanotubes and nanowires using mesoporous templates*, Journal of Physics: Condensed Matter 15 (2003), p.p. 8303-8014

42. N. Petkov, N. Stock, T. Bein, *Gold Electroless Reduction in Nanosized Channels of Thiol-Modified SBA-15 Material*, J. Phys. Chem., 109:21 (2005), p.p. 10737 -10743

43. H. Araki, A. Fukuoka, Y. Sakamoto, S. Inagaki, N. Sugimoto, Y. Fukushima, M. Ichikawa, *Template synthesis and characterization of gold nanowires and particles in mesoporous channels of FSM-16*, J. Mol. Cat. A., 199 (2003), p.p. 95-102.

44. W. Hiroaki, F. Yoshiaki, *Supercritical CO_2 for Making Nanoscale Materials*, Ind. & Eng, Chem. Res., 45:10 (2006), p.p. 3328 - 3331

45. K. B. Lee, S. M. Lee, J. Cheon, *Size-Controlled Synthesis of Pd Nanowires Using Mosoporous Silica Template via Chemical Vapor Infiltration*, Adv. Mater, 13 (2001), p.p. 517-520

46. A. Fukuoka, H. Araki, Y. Sakamoto, S. Inagaki, Y. Fulushima, M. Ichikawa, *Palladium nanowires and nanoparticles in mesoporous silica template*, Inorg. Chim. Acta., 350 (2003), p.p. 371-378.

47. Y. Sakamoto, A. Fukuoka, T. Higuchi, N. Shimoura, S. Inagak, M. Ichikawa, *Synthesis of platinum nanowires in organic-inorganic mesoporous silica templates by photoreduction: formation mechanism and isolation.* J. Phys. Chem. B, 108 (2004), p.p. 853-858.

48. C. M. Yang, H. S. Sheu, K. J. Chao, *Templated synthesis and structural study of densely packed metal nanostructures in MCM-41 and MCM-48*, Adv. Func. Materials 12:2 (2002), p.p.143-148

49. A. Fukuoka, N. Higashimoto, Y. Sakamoto, S. Inagaki, Y. Fukushima, M. Ichikawa, *Preparation, XAFS characterization, and catalysis of platinum nanowires and nanoparticles in mesoporous silica FSM-16*, Topics in Catalysis, 18:1-2 (2002), p.p. 73

50. A. F. Crønsted, Akad. Handl, Stockholm, 18 (1756), p.p. 120 [Source: Cornelis van Laak, A. N., *Post-Synthesis Modifications on Zeolites for Improved Accessibility and Catalytic Performance*, Ph.D. Dissertation (2011), Utrecht University, Netherlands]

51. M. Hódi, K. Polyák, J. Hlavay, *Removal of pollutants from drinking water by combined ion Exchange and adsorption methods, Environmental International*, 21:3 (1995), p.p. 325-331

52. M. W. Ackley, S. U. Rege, S. U., H. Saxena, *Application of natural zeolites in the purification and separation of gases*, Microporous and Mesoporous Materials, 61 (2003), p.p. 25-42

53. D. Mravec, J. Hedec, I. Janotka, *Some Possibilities of Catalytic and Noncatalytic Utilization of Zeolites*, Chem. Pap. 59:1 (2005), p.p. 62-69

54. P. Misaelides, *Application of natural zeolites in environmental remediation: A short review*, Microporous and Mesoporous Materials, 114 (2011), p.p. 15-18

55. H. Nassiri Moghaddam, R. Jahanian, H. Jahanian Najafabadi and M.M. Madaeni, *Influence of Dietary Zeolite Supplementation on the Performance and Egg Quality of Laying Hens Fed Varying Levels of Calcium and Nonphytate Phosphorus*, Journal of Biological Sciences, 8 (2008), p.p. 328-334.

56. A. Dyer, K. Y. Mikhail, *The use of zeolites for treatment of radioactive waste*, *Mineralogical Waste Magazine*, 49 (1985), p.p. 203-210

57. I. Tamane, T. Nakazawa, *Developments of zeolite for non-phosphated detergents in Japan*, Pure & Appl. Chem., 58:10 (1986), p.p. 1397-1404

58. W. Barthel, J. Marchand, M. Von Devivere, *Warm Mix Asphalt by Adding a Synthetic Zeolite*, Proceedings of the Third Eurasphalt and Eurobitume Conference, Book 1, Foundation Eurasphalt, Breukelen, The Netherlands, 2004, p.p. 1241-1249.

59. F. A. Mumpton, *La roca mágica: Uses of natural zeolies in agriculture and industry*, Proc. Natl. Acad. Sci. USA, 96 (1999), p.p. 3463-3470

60. International Zeolite Association: http://www.iza-online.org/

61. J. A., Anderson, M. Fernández García, *Supported Metals in Catalysis*, Imperial College Press, 2005

62. R. J. Davis, *Aromatization on Zeolite L-Supported Pt Clusters*, Heterog. Rev., 1 (1994), p.p. 41-53

63. B. K. Teo, C. P. Li, X. H. Sun, N. B. Wong, S. T. Lee, *Silicon-silica nanowires, nanotubes, and biaxial nanowires: Inside, outside and side-by-side growth of silicon versus silica on zeolite*, Inor. Chem., 42 (2003), p.p. 6723-6728

64. W. Zhou, W., M. J. Edmondson, P. A. Anderson, P. P. Edwards, TEM studies of the in-situ growth of silver metal nanowires from zeolites, Electron Microscopy and Analysis, Inst. Phys. Conf. Ser., 168 (2001), p.p.397-400

65. P. A. Anderson, M. J. Edmonson, P. P. Edwards, I. Gameson, P. Jill Meadows, S. R. Johnson, W. Zhou, *Production of Ultrafine Single-Crystal Copper Wires through Electron Beam Irradiation of Cu-containing Zeolite X*, Z. Anorg. Allg. Chem., 631: 2-3 (2005), p.p. 443-447

66. L. Quiñones, J. Grazul, and M. M. Martínez-Iñesta, *Synthesis of platinum nanostructures in zeolite mordenite using a solid-state reduction method*, Material Lett., 63(2009), p.p. 2684-2686

67. J. A. Huertas-Miranda and M. M. Martínez-Iñesta, *Monte Carlo Simulation Studies for the Templated Synthesis of Ni Nanowires in Zeolites*, Sensors & Transducers J., 7 (2009), p.p. 116-124

68. J. A. Huertas-Miranda and M. M. Martínez-Iñesta, *Si/Al and Metal Loading Effects on the Templated Synthesis of Ni Nanowires in CAN and MOR Zeolite Frameworks*, Molecular Simulation 36: 12 (2010), p.p. 1004-1012

69. J. A. Huertas-Miranda and M. M. Martínez-Iñesta, *Effect of Temperature, Si/Al, and Metal Loading on the Positioning of Pt Atoms in MOR-type Zeolites*, Molecular Simulation, 38:4 (2012), p.p. 300-308

70. M. P. Allen, D. J. Tildesley, *Computer Simulation of Liquids*, Clarendon Press, Oxford, 1987

71. D. Frankel, B. Smit, *Understading Molecular Simulation From Algorithms to Applications*, Academic Press, San Diego, 2002

72. A. R. Leach, *Molecular Modelling Principles and Applications*, Pearson Prentice Hall, Harlow, 2001

73. D. C. Rapaport, *The Art of Molecular Dynamics Simulation*, Cambridge University Press, 2004

74. N. Metropolis, S. Ulam, *The Monte Carlo Method*, Journal of the American Statistical Association (American Statistical Association), 44:247 (1949), p.p. 335–341

75. D. R. Hartree, *The Wave Mechanics of an Atom with a Non-Coulomb Central Field. Part I. Theory and Methods*, Mathematical Proceedings of the Cambridge Philosophical Society, 24 (1928), p.p. 89-110

76. A. Szabo, N. S. Ostlund, *Modern Quantum Chemistry*, Dover Pub., New York, 1996

77. J. C. Slater, *Atomic Shielding Constants*, Physical Review, 36 (1930), p.p. 57-64

78. J. A. Pople, R. K. Nesbet, *Self-Consistent Orbitals for Radicals,* J. Chem. Phys., 22:3 (1954), p.p. 571-572

79. T. H. Dunning, *Gaussian basis sets for use din correlated molecular calculations I. The atoms boron through neon and hydrogen* Chem. Phys. 90 (1989), p.p. 1007-1023

80. P. Hohengberg, W. Kohn, *Inhomogeneous Electron Gas*, Phys. Rev. 136 (1964), p.p. B864-B871

81. L. Sprunch, *Pedagogical notes on Thomas-Fermi theory (and on some improvements): atoms, stars, and the stability of bulk matter*, Rev. Mod. Phys. 63 (1991), p.p. 1512

82. H. Sun, S.T. Mumby, J. R. Maple, and T. Hagler, *Ab Initio calculations on Small Molecule Analogues for Polycarbonates*, J. Phys. Chem. 99 (1995), p.p. 5873-5882.

83. H. Sun, *Ab Initio Calculations and Force field Development for Computer Simulation of Polysilianes*, Macromolecules 78 (1995), pp. 701-712.

84. Literature provided by Accelrys in Material Studio Software (Versions 4.0 and 5.5)

85. J. W. Tester, M. Modell, *Chaper 10 - Statistical Mechanical Approach for Property Models in Thermodynamics and Its Applications (3rd Edition)*, Printence Hall, 1996

86. J G. Vitillo, G. Ricchiardi, G., G. Spoto, A. Zecchina, *Theoretical maximal storage of hydrogen in zeolitic frameworks*, Phys. Chem. Chem. Phys., 7 (2005), p.p. 3948-3854

87. F. Haase, J. Sauer, J. Hutter, *Ab initio molecular dynamics simulation of methanol adsorbed in chabazite*, Chemical Physics Letters 266 (1997), p.p. 397-402

88. A. Gupta, L. A. Clark, R. Q. Snurr, *Grand Canonical Monte Carlo Simulations of Nonrigid Molecules: Siting and Segregation in Silicate Zeolite*, Langmuir, 16 (2000), p.p. 3910-3919

89. C. Tunca, D. M. Ford, *A hierarchical approach to the molecular modeling of diffusion and adsorption at nonzero loading in microporous materials*, Chemical Engineering Science, 58 (2003), p.p. 373-3383

90. M. D. Macedonia, D. D. Moore, E. J. Maginn, *Adsorption Studies of Methane, Ethane, and Argon in the Zeolite Mordenite: Molecular Simulations and Experiments*, Langmuir 16 (2000), p.p. 3823-3834

91. F. Tielens, J. F. M. Denayer, I. Daems, G. V. Baron, W. J. Portier, P. Gerlings, *Adsorption of the Butane Isomers in Faujasite: A combined ab-initio Theoretical and Experimental Study*, Journal of Physical Chemistry B, 107 (2003), p.p. 11065-11071

92. W. J. M. van Well, X. Cottin, B. Smit, J. H. C. van Hooff, R. A. van Santen, *Chain Length Effects of Linear Alkanes in Zeolite Ferrierite, 2. Molecular Simulations*, Journal of Physical Chemistry B, 102 (1998), p.p. 3952-3958

93. A. Goj, D. S. Sholl, E .D. Akten, D. Kohen, *Atomistic Simulations of CO_2 and N_2 Adsorption in Silica Zeolites: The Impact of Pore Size and Shape*, Journal of Phys. Chem, B. 106 (2002), p.p. 8367-8375

94. K.S. Smirnov, F. Thibault-Starzyk, F., *Confinement of Acetonitrile Molecules in Mordenite, A Computer Modeling Study*, Journal of Physical Chemistry B, 103 (1999), p.p. 8595-8601

95. T.H. Demuth, L. Benco, J. Hafner, H. Toulhoat, *Adsorption of Water in Mordenite - An ab-initio study*, International Journal of Quantum Chemistry, 84 (2001), p.p. 110-116

96. J. R. Hill, A. R. Miniham, E. Wimmer, C. J. Adams, *Framework dynamics including computer simulations of water adsorption isotherm of zeolite Na-MAP*, Phys. Chem. Chem. Phys. 2 (2000), p.p. 4255-4264

97. K. Shirono, A. Endo, H. Daiguji, *Molecular Dynamics Study of Hydrated Faujasite-Type Zeolites*, J. Phys. Chem. B, 109 (2005), p.p. 2446-3453

98. M. Fleys, R. W. Thompson, J. C. MacDonald, *Comparison of the Behavior of Water Silicate and Dealuminated Y at Different Temperatures by Molecular Dynamics Simulations*, J. Phys. Chem. B. 108 (2004), p.p. 12197-12203

99. P. Demontris, G. Stara, G. B. Suffritti, *Behavior of Water in the Hydrophobic Zeolite Silicate at Different Temperatures. A Molecular Dynamics Study*, J. Phys. Chem. B 107 (2003), p.p. 4426-4436

100. G. K. Papadopoulos, D. N. Theodorou, *Hierarchical Simulations of Diffusion in Zeolites*, Diffusion Fundamentals 2 (2005), p.p. 1-25

101. A. I. Skoulidas, D. S. Sholl, *Transport Diffusivities of CH_4, CF_4, He, Ne, Ar, Xe, and SF_6 in Silicate from Atomistic Calculations*, Journal of Physical Chemistry B, 106 (2002), p.p. 5058-5067

102. D. F. Plant, M. Guillaume, R. G. Bell, *Diffusion of Methanol in Zeolite NaY: A Molecular Dynamics Study*, Journal of Physical Chemistry B, 111 (2007), p.p. 2836-2844

103. D. Dubbeldam, *Computer-simulation of Adsorption and Diffusion of Hydrocarbons in Zeolites*, Ph.D. Thesis, University of Amsterdam, 2005

104. D. Schuring, *Diffusion in Zeolites: Toward a Microscopic Understanding*, Ph. D. Thesis, Technische Universiteit Eindhoven, 2002

105. V. Iyengar, M. Coppens, *Dynamic Monte-Carlo simulations of binary self-diffusion zeolites: effect of strong adsorption sites*, Chemical Engineering Science, 59:22-23 (2004), p.p. 4747-4753

106. L. Benco, T. Bucko, J. Hafner, H. Toulhoat, *Periodic DFT calculations of the Stability of Al/Si Substituions and Extraframework Zn^{2+} Cations in Mordenite and Reaction Pathway for the Dissociation of H_2 and CH_4*, Journal of Physical Chemistry B, 109 (2005), p.p. 20361-20369

107. K. Teraishi, A. Koichi, A., *Effect of NNN Site Si/Al Substitution on the Acid Strength: Mordenite*, Journal of Physical Chemistry B, 101 (1997), p.p. 1298-1304

108. M. E. Grillo, M. M. Ramírez de Agudelo, *Modeling of Platinum Clusters in H-Mordenite*, Journal of Molecular Modeling, 2 (1996), p.p. 183-189

109. O. Gülseren, F. Ercolessi, E. Tosatti, *Noncrystalline Structures of Ultrathin Unsupported Nanowires*, Physical Review Letters, 80: 17 (1998), p.p. 3775-3778

110. B. Wang, S. Yin, G. Wang, A. Buldum, J. Zhao, *Novel Structures and Properties of Gold Nanowires*, Phys. Rev. Lett., 86:10 (2001), p.p. 2046-2049

111. B. Wang, G. Wang, Y. Ren, H. Sun, X. Chen, J. Zhao, *Electronic and magnetic properties of ultrathin rhodium nanowires*, J. Phys.: Condens. Matter, 15 **(**2003), p.p. 2327-2334

112. C. Peng, J. Gong, L. Wanga, *The structure of ultrathin Ni nanowires*, Computational Materials Science, 46 (2009), p.p. 229–232

113. F. Ercolessi, E. Tosatti, *Au (100) Surface Reconstruction*, Phys. Rev. Lett., 57:6 (1986), p.p. 719-722

114. H. S. Lim. C. K. Ong, F. Ercolessi, *Stability of face-cubic and icosahedral lead clusters*, Surface Science, 269-270 (1992), p.p. 1109-1115

115. Y. H. Luo, J. Zhao, S. Qiu, G. Wang, *Genetic-algorithm prediction of the magic-number structure of $(C_{60})_n$ clusters with a first-principles interaction potential*, Phys. Rev. B, 58:23 (1999), p.p. 14903-14906

116. R. P. Gupta, *Lattice relaxation at a metal surface*, Phys. Rev. B, 23:12 (1981), p.p. 6265-6270

117. S.P. Chen, A.F. Voter, R.C. Albers, A.M. Boring, P.J. Hay, *Investigation of the effects of boron on Ni3Al grain boundaries by atomistic simulations*, Journal of Materials Research, 5 (1990), p.p. 955-970

118. T. Makita, K. Doi, K. Nakamura, A. Tachiban, *Structures and electronic properties of aluminum nanowires*. Journal of Chemical Physics, 119:1 (2003), p.p. 539-545

119. J. C. Zheng, H. Q. Wang, A. T. S. Wee, C. H. A. Huan, *Structural and electronic properties of Al nanowires: an ab initio pseudopotential study*, International Journal of Nanoscience, 1:2 (2002), p.p. 159-169

120. E. Y. Zarechnaya, N. V. Skorodumova, S. I. Simak, B. Johansson, E. I. Isaev, *Theoretical study of linear monoatomic nanowires, dimmer and bulk of Cu, Ag, Ni, Pd and Pr*, Computational Material Science, 2008

121. Y. H. Wen, Z. Z. Zhu, R. Zhu, G. F. Shao, *Size effects on the melting of nickel nanowires: a molecular dynamics study*, Physica E:25 (2004), pp 47–54

122. S. J. A. Koh, H. P. Lee, C. Lu, Q. H. Cheng, *Molecular dynamics simulation of a solid platinum nanowire under uniaxial tensil strain: Temperature and strain-rate effects*, Physical Review B, 72 (2005), p.p. 085414 1-11

123. F. Cleri, V. Rosato, *Tight-binding potentials for transition metals and alloys*, Phys. Rev. B , 48 (1993), p.p. 22-33

124. A. P. Sutton, J. Chen, *Long-range Finnis-Sinclair potentials*, Philos. Mag. Lett. 61 (1990), p.p. 139-164

125. S. W. Lin, S. C. Chang, R. S. Liu, S. F. Hu, N. T. Jan, *Fabrication and magnetic properties of nickel nanowires*, Journal of Magnetism and Magnetic Materials, 282 (2004), p.p. 28-31

126. T.H. Demuth, J. Hafner, L. Benco, H. Toulhoat, *Structural ad Acidic Properties of Mordenite: An ab Initio Density-Functional Study*, J. Phys. Chem. B, Vol. 104, 2000, p.p. 4593-4607

127. P. Gallezot, *Preparation of Metal Clusters in Zeolites*, Molecular Sieves 3, Springer-Verlag, Berlin Heidelberg, 2002

128. Y. Oshima and A. Onga, *Helical Gold Nanotube Synthesized at 150 K*, Physical Review Letters 91:20 (2003), pp 205503-1 - 205503-4

Appendix A - Functional Form and Parameterization of the Polymer Consistent Forcefield (*pcff*)

The Polymer Consistent Forcefield (*pcff*) has the following functional form, which is shared with other forcefields of the same family (cff91, cff, and COMPASS):

$$E_{pot} = \sum_{b} \left[K_2(b-b_o)^2 + K_3(b-b_o)^3 + K_4(b-b_o)^4\right] +$$

term 1

$$\sum_{\theta} \left[H_2(\theta-\theta_o)^2 + H_3(\theta-\theta_o)^3 + H_4(\theta-\theta_o)^4\right] +$$

term 2

$$\sum_{\phi} \left[V_1(1-\cos(\phi-\phi_1^o)) + V_2(1-\cos(2\phi-\phi_1^o)) + V_3(1-\cos(3\phi-\phi_3^o))\right] +$$

term 3

$$\sum_{\chi} K_\chi \chi^2 \quad + \quad \sum_{b}\sum_{b'} F_{bb'}(b-b_o)(b'-b'_o) \quad + \quad \sum_{\theta}\sum_{\theta'} F_{\theta\theta'}(\theta-\theta_o)(\theta'-\theta'_o) \quad +$$

term 4 term 5 term 6

$$\sum_{b}\sum_{\theta} F_{b\theta}(b-b_o)(\theta-\theta_o) \quad + \quad \sum_{b}\sum_{\phi}(b-b_o)(V_1\cos\phi + V_2\cos 2\phi + V_3\cos 3\phi) \quad +$$

term 7 term 8

$$\sum_{b'}\sum_{\phi}(b'-b'_o)[V_1\cos\phi + V_2\cos 2\phi + V_3\cos 3\phi] \quad +$$

term 9

$$\sum_{\theta}\sum_{\phi}(\theta-\theta_o)[V_1\cos\phi + V_2\cos 2\phi + V_3\cos 3\phi] \quad +$$

term 10

$$\sum_{\phi}\sum_{\theta}\sum_{\theta'} K_{\phi\theta\theta'}\cos\phi(\theta-\theta_o)(\theta'-\theta'_o) + \sum_{i>j}\frac{q_i q_j}{\varepsilon r_{ij}} \quad + \sum_{i>j}\left[\frac{A_{ij}}{r_{ij}^9} + \frac{B_{ij}}{r_{ij}^6}\right]$$

term 11 term 12 term 13

Differences between these forcefields are related to the functional groups included, how they were parameterized, and rules for assignment and combination of parameters for non-bond terms.

In this functional form, the first and second terms employ quartic polynomials for bond and angle bending, respectively. The third term uses Fourier expansion for torsions. The out-of-plane (or inversion) coordinate is computed by the fourth term as defined by Wilson et al.. Cross terms up through third order that have been found to have impact on energy calculations are attended by terms 5 to 11. The term 12 is the Coulombic interaction between the atomic charges and term 13 attends the van der Waals interactions, using an inverse 9^{th} power term for the repulsive forces instead of the traditional 12^{th} power term found in Lennard Jones potential.

In addition to polymer and zeolite atom parameterizations, *pcff* include parameters for Li, K, Cr, Mo, W, Fe, Ni, Pd, Pt, Cu, Ag, Au, Al, Sn, and Pb. Parameterizations for the atoms of these metals are done using only the term 13, which has the functional form of Lennard Jones potential.